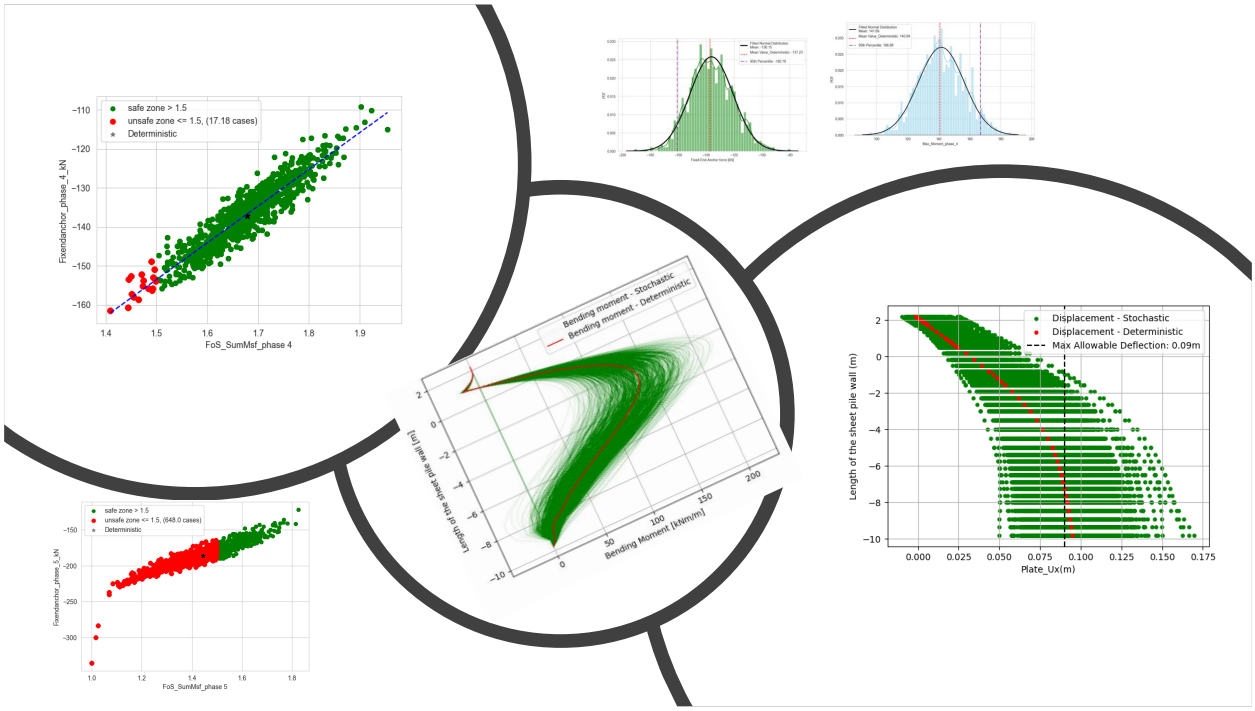

Evaluating the impact of geotechnical uncertainty in deep excavations through probabilistic design

Master's thesis in Infrastructure and Environmental Engineering technology

Pejman Hajibabaei

DEPARTMENT OF ARCHITECTURE
CHALMERS UNIVERSITY OF TECHNOLOGY
Master's thesis ACEX30
Gothenburg, Sweden 2024

Master's thesis ACEX30

Evaluating the impact of geotechnical uncertainty in deep excavation through probabilistic design

Pejman Hajibabaei

CHALMERS
UNIVERSITY OF TECHNOLOGY

Department of Architecture and Civil Engineering
DIVISION OF GEOLOGY & GEOTECHNICS
Chalmers University of Technology
Gothenburg, Sweden 2024

Evaluating the impact of geotechnical uncertainty in deep excavation through probabilistic design

Pejman Hajibabaei

Supervisor at Chalmers: Professor Jelke Dijkstra, Department of Architecture and Civil Engineering
Supervisor at Skanska: Anders Kullingsjö, Skanska Teknik
Examiner: Minna Karstunen, Department of Architecture and Civil Engineering

Department of Architecture and Civil Engineering
Division of Geology and Geotechnics
Chalmers University of Technology
SE-412 96 Gothenburg
Telephone +46 31 772 1000

Cover: An illustration of probabilistic analysis in PLAXIS 2D

Department of Architecture and Civil Engineering
Gothenburg, Sweden 2024

Evaluating the impact of geotechnical uncertainty in deep excavation through probabilistic design

Pejman Hajibabaei
Department of Architecture and Civil Engineering
DIVISION OF GEOLOGY & GEOTECHNICS
Chalmers University of Technology

Abstract

As geotechnical projects increase in complexity, such as deep excavations with embedded sheet pile walls in soft soil, reducing uncertainty and ensuring reliable design become challenging. Misunderstanding the inherent variability of soil properties, such as undrained shear strength and stiffness, can lead to the misestimation of safety margins and structural performance. While traditional hand calculations using partial factors can address uncertainty, they often fall short in complex projects involving different failure mechanisms. In contrast, probabilistic analysis combined with finite element methods offers a more applicable approach for estimating credible failure probabilities and ensuring the reliability of geotechnical design.

The primary purpose of this thesis is to apply a fully probabilistic design approach under a reliability index of three, considering two different coefficients of variation (COV) of 10% and 20%. Additionally, the study investigates the impact of variability in two key clay properties and quantifies the performance of retaining walls with their lateral support components. Lastly, it evaluates the limitations and strengths of the probabilistic design approach compared to traditional hand calculation methods. To demonstrate the benefits of a fully probabilistic design, 2000 random calculations were generated using Monte Carlo simulation in PLAXIS 2D. All generated results were then analyzed and compared with deterministic designs.

The findings indicate that applying 20% COVs increased the predicted range of the wall's maximum bending moment, waler force, and horizontal deflection, showing a broader response. The significant effect of traffic loads combined with higher soil variability resulted in high wall deflection and lower factors of safety in the majority of realizations. The convergence of deterministic and probabilistic designs underscores the importance of applying probabilistic methods to achieve more reliable and uncertainty-informed geotechnical designs.

Keywords: Probabilistic design, reliability based design, coefficient of variations, soil variability, Monte Carlo simulations, random FEM, deep excavation, sheet pile wall

Acknowledgements

I had a great journey in my thesis, a journey filled with all sorts of emotions, from deepest level of frustration to the highest level of enjoyment and happiness. During my journey, there were people who supported me.

I would like to express my deepest gratitude to my dear wife, Hadjar, for her encouragement, patience and love, which were a great source of motivation for me.

I would also like to extend my greatest appreciation to my supervisor, Jelke Dijkstra, at Chalmers University of Technology. Thank you for your guidance, dedication, and support, not only during my thesis but throughout my entire journey at Chalmers University.

Furthermore, I would like to express my gratitude to my supervisor, Anders Kulingsjö, at Skanska Teknik. Thank you, Anders, for all the interesting conversations, your practical insights, your guidance, and your encouragement to push the limits of geotechnical engineering.

To all those mentioned, your contributions have been the most important and essential to feeling the success and improvement. Thank you all!

Pejman Hajibabaei, Gothenburg, June 2024

Contents

List of Figures

List of Tables

addcontentsline

Symbol	Description
A_w	Cross sectional area [mm^2]
β	Reliability index [-]
c_0	Cohesion [kPa]
COV	Coefficient of variation (COV = $\frac{\sigma}{\mu}$)
E	Structural or soil stiffness (Young's Modulus) [kPa]
EI	Bending stiffness [kNm^2/m]
γ	Volumetric weight [kN/m^3]
γ_{unsat}	Volumetric weight of unsaturated soil [kN/m^3]
γ_{sat}	Volumetric weight of saturated soil [kN/m^3]
γ_m	Material partial factor [-]
σ	Standard deviation
$M_{DA3,1}$	Maximum bending moment without unfavorable load
$M_{DA3,2}$	Maximum bending moment with unfavorable load
M	Bending moment [kNm] or [kNm/m]
C_u	Undrained shear strength or cohesion
μ	Mean value
FoS	Factor of safety [-]
n	Number of random variables
CPT	Cone Penetration Test
τ	Shear strength
δ_h	Maximum permissible displacement of the wall
U_x	Total lateral wall deflection in x direction
P_f	Probability of failure
MC	Mohr-Coulomb soil model
$FORM$	First order reliability method
$FOSM$	First-Order Second Moment Reliability Method
PDF	Probability density function
CDF	Cumulative Distribution Function
MCS	Monte Carlo Simulation
R	Resistance
S	Load
σ	Standard deviation
σ^2	Variance
x	Evaluation points
X	Soil property
ULS	Ultimate Limit State
SLS	Serviceability Limit State

1

Introduction

Ensuring safety and estimation of uncertainty in geotechnical engineering is undeniably important. Stability and safety of geotechnical structures can be depended on effect of inherent soil variability. In many years, traditional deterministic design methods have been used for solving many geotechnical problems, offering easy-to-use approaches for design. However, these methods do not account for inherent soil variability. Modeling problems such as retaining walls in soft clay require accurately analyzing structural responses corresponding to soil variability. To address this challenge and ensure overall safety in design, geotechnical engineers utilize predefined partial factors as outlined in Eurocode 7, which aim to mitigate uncertainties when site investigation data is insufficient. Recent studies demonstrate that larger partial factors may not guarantee safety in geotechnical design.

Understanding the randomness in soil parameters and errors in measurement during site investigations highlights the necessity to utilize probabilistic approaches to quantify the magnitude of uncertainty and adapt the design process to develop robust solutions. Traditional approaches are not able to capture the uncertainty present in soil and loading conditions, which is critical for complex projects such as deep excavations in soft clay with different failure modes. However, with advancements in geotechnical finite element methods, it is now possible to capture the complex interaction of structural elements and soil. Combining finite element methods with probabilistic approaches, such as Monte Carlo simulation, enables geotechnical engineers to quantify the reliability of their designs and provide detailed insights into the impact of soil variability on the performance of retaining structures in deep excavations.

The primary purpose of this thesis is to investigate the performance of sheet pile wall using a combination of finite element methods and probabilistic approaches. This study focuses particularly on the variability of soft clay's undrained shear strength and stiffness under two different levels of uncertainty. By assessing how different levels of uncertainty influence the geotechnical factor of safety and the performance of the sheet pile wall. Additionally, this thesis aims to provide a comparative analysis that highlights the strengths and limitations of each design approaches. To present a comprehensive comparison between deterministic and probabilistic approaches, this thesis employs a literature review and simulations performed by finite element method, considering coefficients of variation (COV) of 10% and 20% for two soil variables.

1.1 Aim

The aim of this thesis is based on investigating opportunities of using probabilistic analysis in geotechnical finite element analysis. The study performs multiple finite element realizations based on software program PLAXIS 2D. the main goals of study are expressed as:

- Quantifying the impact of soil variability on performance of embedded sheet pile wall, in deep excavation in soft clay.
- Assess the difference of reliability-based design used Monte Carlo simulation compared to single deterministic design.

1.2 Objectives

1. Implement probabilistic finite element analysis (level III) in PLAXIS 2D for a deep excavation in soft clay.
2. Present the impact of different degree of uncertainty COV 10% and COV 20% on wall deflection, waler forces, bending moment and check the geotechnical failure by evaluating factor of safety.
3. Assess the material factors used in design, i.e. level II against the results of a level III analysis for a relevant idealized case of a deep excavation in soft soil.
4. Evaluate the system reliability of the design and provide suggestions to mitigate the risks and optimization of the design process.

1.3 Limitations

This thesis has its own limitations which are outlined as it follows:

- All simulations were performed as an undrained (total stress analysis), hence the delayed time effects such as consolidation, weathering and creep were not considered.
- 3D and geometrically non-linear effects are not considered. Simplified continuous sheet pile wall and its structural elements is considered. Friction in lock between sheet pile walls and buckling effect for waler/ strut were neglected.
- For calculation of wall deflection, the effect of concrete slab on excavation bottom was excluded in all simulations. In reality the project performed by stepwise excavation with building concrete slab which can reduce the deflection of the wall.

2

Theory

This chapter presents a literature study aimed at enhancing the comprehension of probabilistic-based design in geotechnical engineering. The connection between geotechnical engineering and probabilistic design necessitates a foundational understanding of the uncertainties inherent in soil properties, stability analysis, limit states, and the critical factors influencing retaining structures (K. Phoon & J. Ching, 2015). It delves into the details of performance functions and numerous other aspects involved in the design process.

2.1 Geotechnical Uncertainty

Uncertainty is often coupled to risk related to a high probability of failure. There is no doubt that there is randomness in the soil and there is variability; when there is variability, so there is error in the accuracy and reliability of the estimation of soil properties. The variability of soil is the inherent property of soil generated through geological processes (Phoon & Kulhawy, 1999a). Moreover, site-specific conditions make it more challenging to quantify the inherent variability and its influence on the uncertainty of soil properties. As Phoon (1990) clarifies, there are several factors that influence overall uncertainties, such as the absence of relevant data, measurement errors generated by various sources such as random testing, inaccuracy of equipment, and even the methods used for conducting measurements (see figure 2.1).

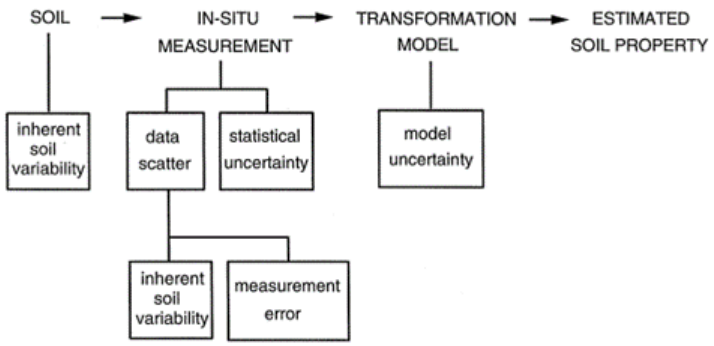

Figure 2.1: Different source of uncertainty in predicting the property of soil (Kulhawy, 1992).

2.1.1 Natural Variation

Variability in environmental, geological, and physicochemical processes of soil makes geotechnical engineering complex. Additionally, the ongoing modification of soil properties due to in-situ conditions can cause variation in vertical and horizontal dimensions(Phoon & Kulhawy, 1999a). the natural variation in soil can be demonstrated by equation 2.1:

$$\xi(z) = t(z) + w(z) \tag{2.1}$$

Where $\xi(z)$ is the in-situ soil property that varies with depth, $t(z)$ represents the trend function, and $w(z)$ is the fluctuation component representing the inherent variability in soil. Before utilizing the equation above, it is necessary to consider that there are two as assumptions to be made: first, if $w(z)$ is statistically homogeneous, the mean and variance of w are not allowed to vary throughout the depth. Secondly, the relationship between differences at two depths is influenced by the distance between them, not their absolute positions (Phoon & Kulhawy, 1999a).

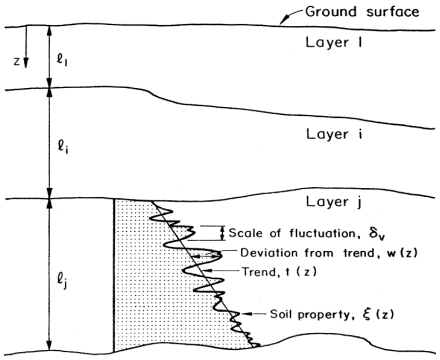

Figure 2.2: Variability in soil through the depth (Kulhawy, 1992)

To assess the inherent variability of soil, there is another significant form of variability in soil known as the scale of fluctuation in the vertical direction, which can be approximated by equation 2.2.

$$\delta_v \approx 0.8d \tag{2.2}$$

Where δ_v is the vertical scale of fluctuation, and as Figure below illustrates, d represents the mean distance related to the points where the fluctuating property intersects with the trend function (Phoon & Kulhawy, 1999a).

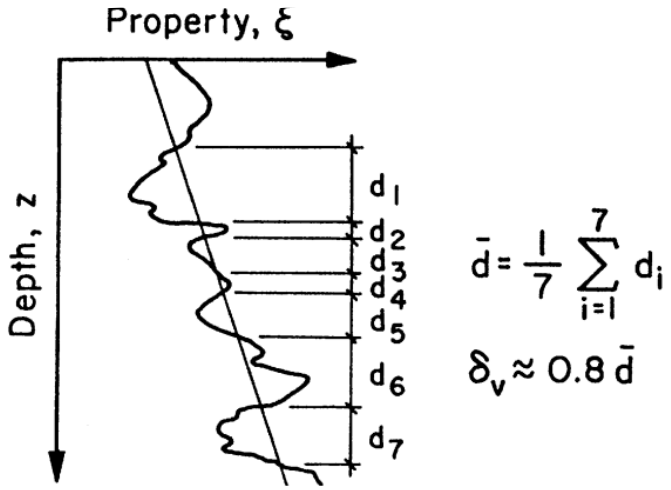

Figure 2.3: Fluctuation property, the vertical scale and its trend line (Spry et al., 1988).

Phoon (1999) has collected data shown in table 2.1 , which estimates the scale of fluctuation in both horizontal and vertical directions for common soil properties. This table is based on an extensive literature review, which illustrates that, for example, the vertical scale of fluctuation for clay's undrained shear strength (Su) can be as low as 0.8 meters and as high as 6 meters. However, the horizontal scale of fluctuation appears to differentiate more than one order of magnitude compared to vertical fluctuation. As table below shows the Su (VST) can fluctuate each 50 meter in x direction compared to vertical fluctuation by each 2.5 meter. It can be considered that the variability in soil parameters is larger in the vertical direction than in the horizontal direction. However, it should be highlighted that the scale of fluctuation presented in table 2.1 can be highly biased by the number of sampling points and it's sampling intervals (Phoon & Kulhawy, 1999a).

Table 2.1: Collected data of scale of fluctuation for different geotechnical properties (Phoon et al. 1995, p. 4-20).

Property[a]	Soil type	No. of studies	Scale of fluctuation (m) Range	Mean
Vertical fluctuation				
s_u	Clay	5	0.8–6.1	2.5
q_c	Sand, clay	7	0.1–2.2	0.9
q_T	Clay	10	0.2–0.5	0.3
s_u(VST)	Clay	6	2.0–6.2	3.8
N	Sand	1	—	2.4
w_n	Clay, loam	3	1.6–12.7	5.7
w_L	Clay, loam	2	1.6–8.7	5.2
$\bar{\gamma}$	Clay	1	—	1.6
γ	Clay, loam	2	2.4–7.9	5.2
Horizontal fluctuation				
q_c	Sand, clay	11	3.0–80.0	47.9
q_T	Clay	2	23.0–66.0	44.5
s_u(VST)	Clay	3	46.0–60.0	50.7
w_n	Clay	1	—	170.0

[a] s_u and s_u (VST), undrained shear strength from laboratory tests and vane shear tests, respectively; $\bar{\gamma}$, effective unit weight.

2.1.2 Transformation Uncertainty

As it mentioned, one of the source errors is methods used conducting measurements. When all measurements from the laboratory are transformed to theoretical or semi-empirical models, transformation uncertainty arises. As an example, if local data for determining undrained shear strength from site investigations are not sufficiently available, transformation models (see equation 2.3) can be utilized to estimate data based on another set of data captured, for instance, from CPTU tests. Using measured undrained shear strength (Su) from CPTU tests to predict Su can contain some epistemic uncertainty which was not considered in the prediction of correct Su (Phoon & Kulhawy, 1999b).

$$Nk = \frac{q_t - \sigma_{v0}}{S_u} \approx c \tag{2.3}$$

Where Nk is the cone factor, q_t is the corrected cone resistance, σ_{v0} is the in-situ vertical total stress, and c is the empirical constant. There is no doubt that the value of c is highly site specific, and it is depended on to other variables, likewise past studies have shown a variance in the empirical constant c, from 8 to 29, which can show the difference in results based on site locations. Overestimation or underestimation of the true undrained shear strength can arise when transformation models cannot take into account multiple important factors such as pore water pressure or overconsolidation ratio (OCR), which is highly correlated to the void ratio from local site investigations. Figure 2.4 illustrates the concept of inherent soil changeability by showing the discrepancy between predicted value of undrained shear strength (Su,pred) against the real measured values (Su,m) at the local site named Drammen (Ching et al., 2016)

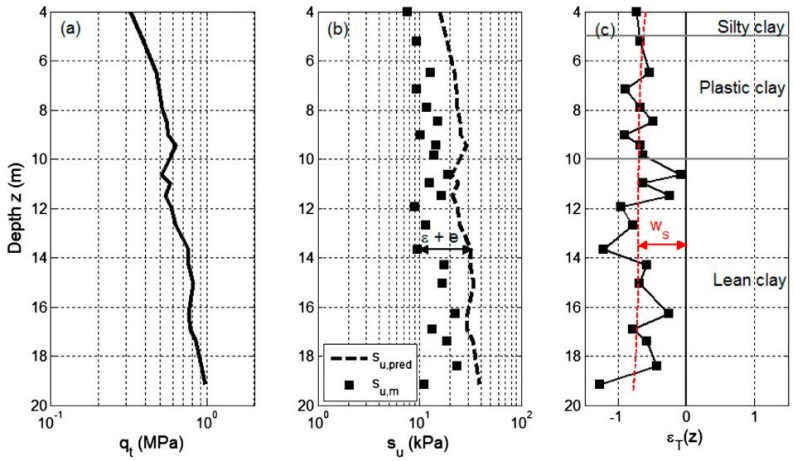

Figure 2.4: The Drammen site(a)cone tip resistance through the depth(z), (b) undrained shear strength measured (Su,m) and predicted (Su, pre), (c) transformation uncertainty compared with measured undrained shear force(Ching et al., 2016).

2.2 Coefficient of Variation (COV)

In the absent of sufficient amount of data related to soil and site-investigations or a lack of detailed analysis, it can be helpful to use a general guideline that estimates the range of variability of soil properties. Moreover, it can be beneficial to have enough site-specific data to combine it with general guidelines by using a technique called Bayesian updating (Phoon & Kulhawy, 1999a). By understanding the underlying concepts of standard deviation and mean, a new concept known as the coefficient of variation (COV), or the degree of uncertainty in site understanding, can be introduced. Geotechnical engineers can recognize the unusual variability of soil properties, which might impact their understanding of the project. The inherent soil variability, as explained by the COV, is a statistical metric and is expressed as a percentage. As equation 2.4 shows, COV is calculated by dividing the standard deviation by the mean for measured values in site-investigation, such as the friction angle or undrained shear strength of the soil.

$$COV = \frac{\sigma}{\mu} \tag{2.4}$$

Where σ is the standard deviation, which shows how much the values in a dataset are differentiated from the mean (Equation 2.5), and μ is the mean (average), which is the sum of all data points divided by the total number of data points in the dataset.

$$\sigma = \sqrt{\frac{1}{n-1}\sum_{i=1}^{n}[w(z_i)]^2} \tag{2.5}$$

Various soil properties have their own coefficient of variations which some of them are collected from a large number of test results, and are available in table 2.2 . It is important to note that the COV values for undrained shear strength in this study was selected based on values reported in literature as summarized in table below (Phoon & Kulhawy, 2008).
The influence of degree of uncertainty in soil variability can have a larg impact on behavior of retaining structures. Past studies showed that by selecting a higher COV value, for instance selecting COV 30% can have relatively higher impact on bending moment and wall deflection compared to lower COV equal to 10%. The reason is that higher COV value generate larger mean value of max bending moment and wall deflection. As result, by choosing higher COV value, the geo-system tends to shift to higher level of uncertainty. Although, by choosing the lower bound (COV 10%), it can lead to reducing the large variation of soil properties and decrease the uncertainty for predicting maximum lateral wall deflection or wall's bending moment(Sert et al., 2016).

2.3 Statistical definition of deterministic design

In the deterministic design, the characteristic values for soil properties, utilizes fixed predetermined input parameters to ensure conservative design for serviceability lim-

Table 2.2: Three different soil properties with three ranges of COVs for three classes.

Geotechnical parameter	Property variability	COV (%)
Undrained shear strength	Low[a]	10–30
	Medium[b]	30–50
	High[c]	50–70
Effective stress friction angle	Low[a]	5–10
	Medium[b]	10–15
	High[c]	15–20
Horizontal stress coefficient	Low[a]	30–50
	Medium[b]	50–70
	High[c]	70–90

Source: Table 9.7; Phoon and Kulhawy (2008).
[a]Typical of good quality direct lab or field measurements.
[b]Typical of indirect correlations with good field data, except for the standard penetration test (SPT).
[c]Typical of indirect correlations with SPT field data and with strictly empirical correlations.

its. As an example, in the case of clay's undrained shear strength, the single deterministic value is usually specified by the mean value for each clay layer. However, it should be highlighted that, deterministic design does not consider the probability of failure and even the inherent uncertainties in soil behavior. Deterministic design favoring a singular, conservative outcome over a probabilistic risk assessment of possible outcomes. It is mentioned In Eurocode-7 that deterministic design should be selected conservatively. Moreover, when dataset is restricted to few data points, the characteristic values chosen using a probabilistic approach should not exceed the 5th percentile. This requires that the estimation of mean characteristic value must at least satisfy the 95% confidence interval ensuring minimum reliable outcome without using partial factor (Hicks, 2012, p. 36). However, It is important to note that, Hicks mentioned that 5% threshold is devoted to having potential failure in structure not to parameter value.

2.3.1 Probability Density Function (PDF)

Understanding the probability of an event occurring based on variable's continuous values within a distribution is vital in statistical analysis. The aggregated distribution generated by many realizations can be termed as a Probability Density Function (PDF). In this distribution x-direction, cover a range from negative to positive values, and in the y-direction, indicates the probability of the occurrence of a value, which can be depicted by two different distribution forms: normal and log-normal. The PDF of lognormal has zero as a minimum value and shifts only toward positive values. The log-normal distribution has been utilized commonly in geotechnical engineering (Zhang et al., 2023, p. 21). Normal and lognormal equations 2.6 and 2.7 can be expressed as:

$$f(x) = \frac{1}{\sqrt{2\pi}\sigma_x} \exp\left[-\frac{(x-\mu_x)^2}{2\sigma_x^2}\right] \tag{2.6}$$

$$f(x) = \frac{1}{\sqrt{2\pi}\sigma_x x} \exp\left[-\frac{(\ln x-\mu_x)^2}{2\sigma_x^2}\right] \tag{2.7}$$

Where X is the random variable, μx is mean value and σ_x is the standard deviation. Figure 2.5 shows an example of different mentioned distributions for undrained shear strength on the x-axis. Figure 2.6, present that when the bell curve is narrow towards the mean value, it can signifies the role of three different COV values on generated mean value of undrained shear strength(K.-K. Phoon & J. Ching, 2015, p. 137)

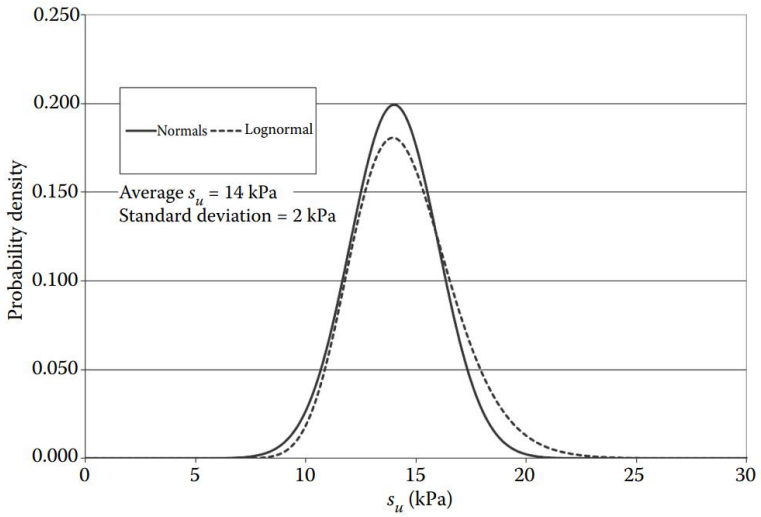

Figure 2.5: Difference between normal and lognormal distribution correspond to PDF (K.-K. Phoon J. Ching, 2015, p. 138)

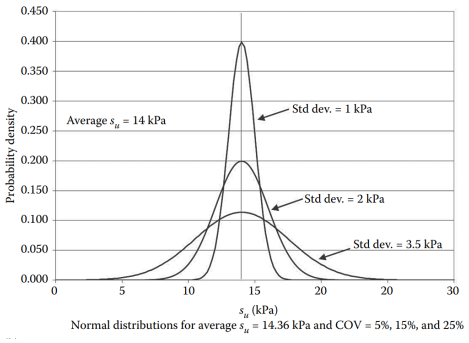

Figure 2.6: The influence of three different coefficient of variations 5%, 15% and 25% on undrained shear strength with mean of 14 kPa(K.-K. Phoon J. Ching, 2015, p. 138)

2.3.2 Cumulative Density Function (CDF)

Another common distribution is cumulative density function distribution illustrates the area under the PDF curve, explaining that the CDF is the integral of the PDF. The dotted lines, representing the CDF in figure 2.7, demarcate the range of undrained shear strength from zero to 30 kPa along the x-axis. On the y-axis, to the right, it is demonstrated that the probability of the occurrence of shear strength less than or equal to 12 kPa is quantified at 13% (K.-K. Phoon J. Ching, 2015, p. 141).

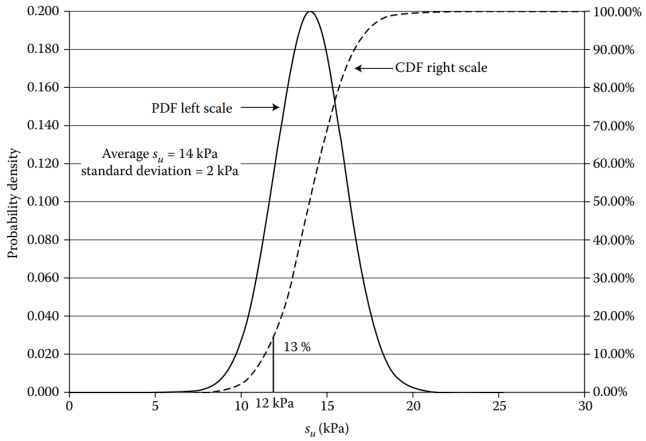

Figure 2.7: Comparing the scale of PDF with CDF for undrained shear strength.

In the figure 2.8, visualize an example that present a critical relationship between the probability of failure, and factor of safety which ranging from an unsatisfactory value 0.50 to a satisfactory 2.5, depicted by the Cumulative Distribution Function (CDF). This graphical representation illustrates that there is only a 1.5% probability of obtaining a factor of safety equal to or less than 1. Moreover, geotechnical engineers can quantify the possibility of having different factor of safety in design by employing CDF distribution.

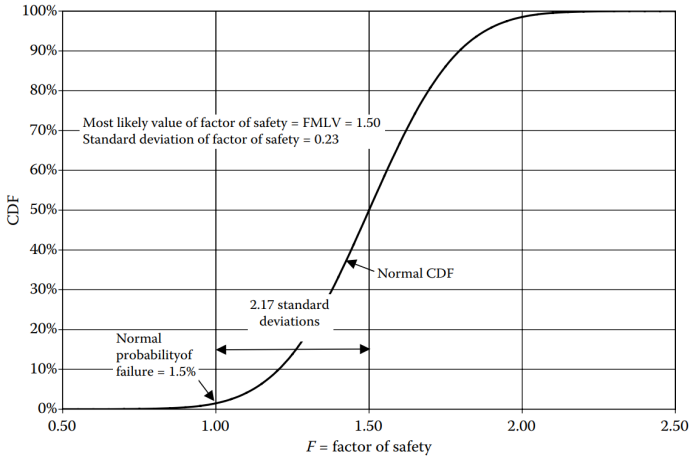

Figure 2.8: Demonstrating an example of probability of having a factor of safety below 1.00(K.-K. Phoon J. Ching, 2015, p. 144)

2.4 Monte Carlo simulation (MCS)

The Monte Carlo Simulation (MCS) is the simplest numerical method for generating a sufficient number of random samples to achieve the desired level of precision. By generating random variable/ variables and conducting numerous repetitions ranging from at least 1000 times upwards, establish distribution of different outcomes based on the random variable(s). Utilizing the MCS methodology empowers geotechnical engineers to explore a range of possible outcomes, which can be categorized into the worst case, or more appropriately, the worst credible and the best credible outcome, rather than focusing on single deterministic design or prescribed partial factors (Honjo, 2008).
The MCS method has been widely employed in many geotechnical analyses and designs based on extensive number of realizations. However, large number of iterations in MCS, can leads to extensive computation time for producing reliable outcomes. The random variable generated by the MCS method can be utilized to assess the performance of the system in the form of geotechnical failure or structural failure. Consider that $\mathrm{X} = [\mathrm{X}_1, X_2, X_3, \ldots, X_n]$ represents a range of uncertain variables and G(X)<0 as a performance function. If for instance the load is higher than resistance the performance function falls below zero and a failure occurs. In this method, it is even possible to calculate the probability of failure and it can be calculated by equation 2.8 (Honjo, 2008).

$$P_f = \frac{1}{N} \sum_{j=1}^{N} I[G(X) < 0] \tag{2.8}$$

Where $I[.]$, is the indicator function and N is the total number of simulations. Suppose there are 1000 Monte Carlo realizations, and only 10 realizations out of 1000 randomly generated realizations resulted in a safety factor less than one. It can be concluded that, based on 1000 random realizations, the probability of failure

is 10 divided by 1000, or 1% (Low, 2008).
An example depicted in the figure 2.9, a blue dotted line represents the performance function for the generated random samples, in this case, friction angle and cohesion. There are a few samples $g(c, \phi) \leq 0$, represented by black dots (failure samples), throughout all sample points that violate the limits of the functions (Zhang et al., 2023, p. 104).

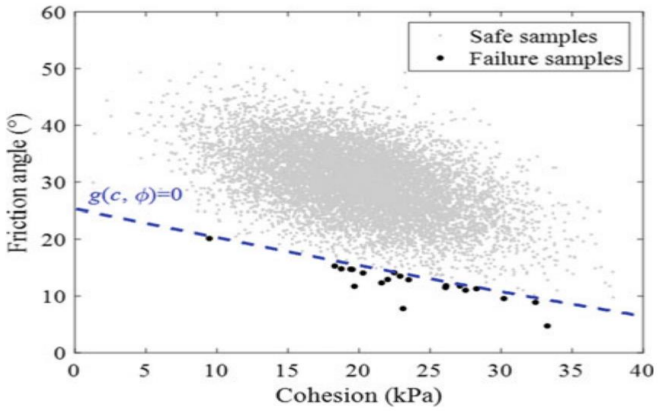

Figure 2.9: Scatter plot of Cohesion (Kpa) and friction angle, showing the few failure samples among 10000 generated samples by MCS(Zhang et al., 2023)

2.5 Virtual site data

The primary goal of generating random variables for soil parameters is to closely replicate the data obtained from actual site investigations. Virtual site data primarily aims to simulate real-world data to better understand the complex interactions between soil and structures. However, it is important to note that virtual site data are not proposed to replace the actual geotechnical and site investigations data; instead, they are designed to augment the partial information obtained from actual sampling. By increasing the number of data points, virtual site data can help geotechnical engineer to enhance accuracy and improve realism during design process. Consequently, information gained by virtual data can lead to having better perspective in reliability-based design and it can serve as a complementary tool in the decision-making process (Ching & Phoon, 2015).

2.6 Reliability Analysis

In geotechnical analysis safety is a vital factor. In contrast with prescribed factor of safety in Eurocode 7 in reliability analysis, there is probabilistic safety analysis involved. In probabilistic approach the level of risk or probability of failure can be assessed even by using reliability index β. This index can be differentiated between ultimate and serviceability limit sates. Reliability index is intrinsically linked to P_f, the probability of failure. In essence, the question focusses on the likelihood of

achieving a reliable design, which equates to 100% minus the probability of failure in designing geosystems, shown in equation 2.9 (Zhang et al., 2023).

$$P_f = \Phi(-\beta) \tag{2.9}$$

Where Φ is cumulative normal distribution. Each specific reliability indices can be linked to the specific range of likelihood of failure (P_f) which is presented in table 2.3 (K.-K. Phoon & J. Ching, 2015, p. 143).

Table 2.3: Summary of reliability index(β) linked to it's probability of failure P_f.

Reliability index β_{Normal} *or* $\beta_{Lognormal}$	*Probability of failure,* P_f
0.50	31%
1.00	16%
1.50	6.7%
2.00	2.3%
2.50	0.62%
3.00	0.13%
4.00	0.003%
5.00	0.00003%

2.7 Reliability methods

Reliability methods in engineering are systematic approaches used to assess the safety and performance of structures and systems, considering the uncertainties inherent in material properties, environmental conditions, and loading forces. As it is presented the exact prediction of performance of the geo-system is not realistic and this is the reason why these methods quantify the probability of failure or unsatisfactory performance, enabling engineers to design more robust and dependable systems(Orr & Breysse, 2008). Figure 2.10 is presenting a schema of different methods for deterministic and probabilistic methods followed by description of several key reliability methods.

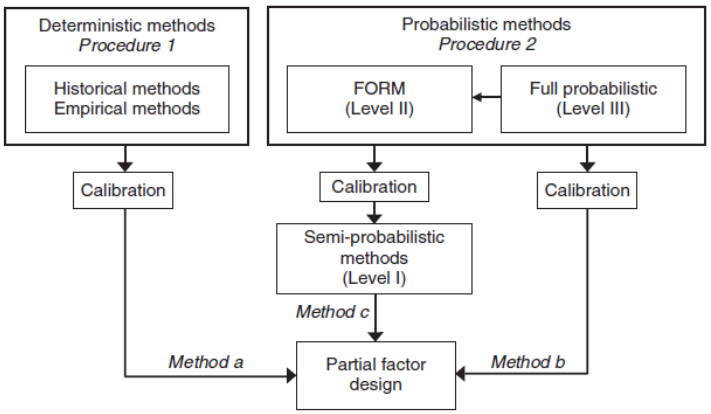

Figure 2.10: Summary of reliability based methods used in Eurocodes(Orr Breysse, 2008).

2.7.1 First order reliability method (FORM)

As highlighted, uncertainty within the scope of geotechnical engineering is pronounced, representing the system vulnerable when attempting to predict behavior through single deterministic designs only. To adequately quantify uncertainty in the performance of geosystems, the probability of risk associated with failure must be assessed. In FORM approach, it is presumed that load and capacity are lognormal distributed thereafter safety can be measured by how likely is that the performance of geo-systems fall under the defined limit (Orr & Breysse, 2008).

2.7.2 Level I (semi-probabilistic design)

The first level of reliability is dedicated to scenarios where an uncertain parameter is assigned a single characteristic value. In level one approach, a partial factor is applied directly to the characteristic value.

2.7.3 Level II

Mean and standard deviation In Level II reliability analysis are the two values assigned to uncertain parameters, which are assumed to be normally distributed. The First-Order Second Moment Reliability Method (FOSM) serves as an appropriate example of Level II analysis. This is a crucial step in determining which reliability method to employ for approximating the likelihood of failure. The FOSM method approximates the probability of failure by amalgamating the mean and standard deviation of input parameters. This is achieved through the utilization of first-order terms of the Taylor expansion, which serves to assess the system's reliability within uncertainty.

2.7.4 Level III (fully probabilistic design)

Level III is aimed to apply more advanced probabilistic models to describe the variability of input variables. Fully probabilistic models or level III can be conducted in a way to identify the critical factors that might the reliability of the design. Monte Carlo simulation can be desirable example for solving geotechnical problems in level III.

2.7.5 System reliability and reliability target

Deep excavation is belonged to one of the critical engineering problem due to the fact that retaining structures can have more than one failure modes. Consequently, reliability of the geo-system can be analyzed rather than analyzing considering solely on a single failure mode. System reliability analysis enables the simultaneous consideration of various interconnected failures, such as lateral sliding, overturning, and soil mass failure beneath the retaining wall. Analysis used Monte Carlo simulations are particularly suited for addressing system reliability issues. This is for the reason that Monte Carlo-based methods generate random realizations, to provide viable and, most critically, unbiased predictions of system behavior. System reliability can be quantified through a reliability index, when higher level of reliability index indicates to safer design(Wang et al., 2016). Tables 2.4 present various levels of reliability indexes as outlined in different expected performance level.

Table 2.4: Examples of expected performance correspond to their reliability index and the likelihood of failure (Duncan, 2000).

Reliability Index β	*Failure Probability* $p_f = \Phi(-\beta)$	*Expected Performance Level*
1.0	0.16	Hazardous
1.5	0.07	Unsatisfactory
2.0	0.023	Poor
2.5	0.006	Below average
3.0	0.001	Above average
4.0	0.00003	Good
5.0	0.0000003	High

Note: $\Phi(\cdot)$ = standard normal cumulative distribution function.

Moreover, it can be observed that targeting reliability index should include the consequences of failures such as environmental, social and economic losses. Table 2.5 provide some examples for different limit states which can reveal that target index β_t varies as project and designs varies(Wang et al., 2016).

Table 2.5: Target reliability index (β_t) in different design codes for two different limit states (Fenton et al., 2015).

Design Code	*ULS* β_t	*SLS* β_t
Electric Power Research Institute (EPRI) multiple resistance and load factor design (MRFD)	3.2	2.6
Canadian Highway Bridge Design Code (CHBDC 2014)	3.1–3.7	2.3–3.1
Canadian National Building Code (NCBC)	3.5	Not available
American Association of State Highway and Transportation Official (AASHTO) foundation design code	2.0–3.5	Not available
Eurocode 7*	4.7	2.9

2.8 Mohr-coulomb model (MC)

The Mohr-Coulomb (MC) model serves as a fundamental tool for approximating the linear behavior of soil, involving both elastic and perfectly plastic ranges (Labuz & Zang, 2014). As it is shown in figure 2.11, MC model delineates failure criteria through two principal strength parameters: the friction angle(ϕ) and cohesion (c), making it well-suited for projects involving shallow foundations, slopes, and embankments (Lees, 2016). In this model, failure occurs when the stress path, represented by the half-circle of $-\sigma_3$ and $-\sigma_1$, intersects with the failure envelope on the Mohr diagram, a relationship shown as a straight line in figure 2.11 It is essential to highlight that in this study, the friction angle is set to zero, thereby directing attention to the soil's behavior under these conditions. Undrained shear strength can be estimated by equation 2.10.

$$\tau = c \tag{2.10}$$

For the analysis of undrained behavior, it is crucial to employ undrained shear strength while setting the friction angle to zero. Nonetheless, the MC model is subject to limitations; notably, it cannot accurately represent the hardening and softening behavior of normally consolidated or softly consolidated soils (Lees, 2016).

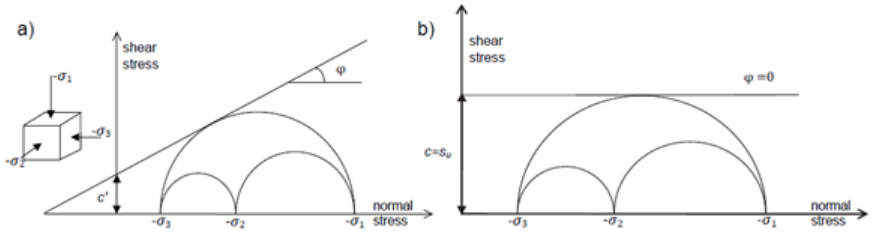

Figure 2.11: Mohr-Columb's envelop (a) Using friction angle for strength parameters (b) Using undrained shear strength with friction angle equal to zero (Brinkgreve, 2007)

2.9 Impact of shear strength and stiffness of the soil in deep excavation

The shear strength and stiffness of soil are undeniably crucial for assessing the overall performance of an excavation project. In the context of short-term excavations in soft clay, the focus often shifts to the undrained behavior of clay, which is typically determined through various laboratory tests, such as the triaxial test, or field evaluations corresponding to the Cone Penetration Test (CPT) (Kempfert, 2006). The undrained behavior of clay is affected significantly by factors including water content and it's stress history. Notably, in normally and slightly overconsolidated clay deposits, the undrained strength is a linear function of depth.

2.10 Retaining system

2.10.1 Sheet pile wall

To retain lateral soil movement during basement excavations, retaining walls are necessary. A prime example of such a structure is the embedded sheet pile wall, commonly driven into the ground via vibration. A distinctive attribute of sheet pile walls is their interlocking capability, enhancing their utility as effective water barriers. Mainly crafted from steel, these walls are frequently designed in U and Z formations, as depicted in figure 2.12, marking them as prevalent choices for excavation projects (Ou, 2021).

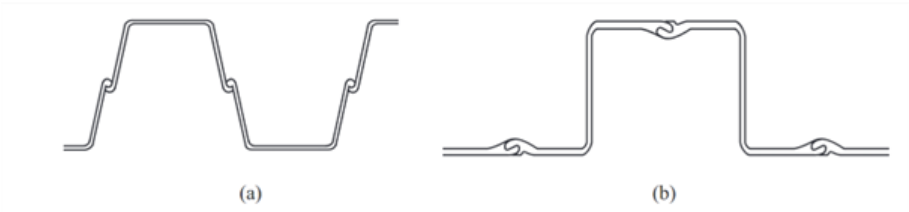

Figure 2.12: Two common steel sheet piles (a) U-pile (b) Z-pile.

Sheet pile walls offer notable advantages, including reusability and efficacy as water barriers. However, they are not without drawbacks: they exhibit lower stiffness relative to column and diaphragm piles, may present challenges during installation in hard soils, and can produce considerable vibration and noise upon installation (Ou, 2021).

2.10.2 Influence criterions on sheet pile wall

For designing retaining structure both short-term and long-term behavior must address a range of possible failures, including general stability, sliding, wall rotation, struts buckling, overstress of retaining components and other factors, illustrated in figure 2.13 (Kempfert, 2006).

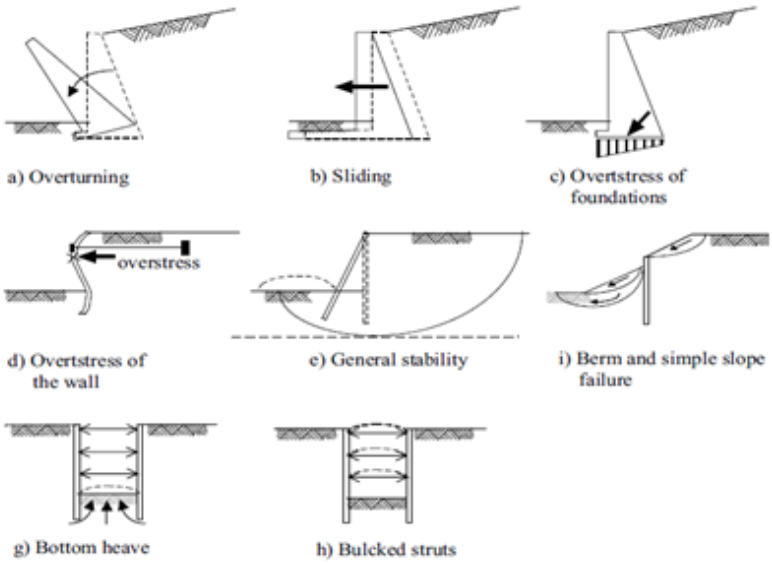

Figure 2.13: Different failures in supported excavations (Kempfert, 2006, p. 127).

The design of retaining structure is governed by many factors such as bending moment on wall. Excessive displacement of backfilled soil, can lead to significant deformations in sheet pile wall, potentially resulting in excessive bending moment. A critical material strength parameter is the wall's maximum allowable bending moment prior to permanent deformation.

2.10.3 Lateral support

Analysis the lateral stability of the retaining sheet pile wall is belonged to another important factor that impact the retaining wall. Soft soils compared with other sort soils respond to surcharge loads such as traffic load more sensitively. Therefore, for excavation in soft soil it is important to provide more safety by anchorage to the base or concrete slab (Kempfert, 2006).

2.10.4 Displacement of wall in horizontal direction

Deformations in sheet pile walls can exhibit when the soil behind the wall lacks adequate strength, or when the supporting components such as anchors, walers, and struts, do not possess the required stiffness to sustain the system. The stiffness of the soil, especially near the wall's toe, predominantly dictates the magnitude of horizontal movement (Kempfert, 2006).
The maximum permissible displacement of the wall in the x-direction is contingent upon the excavation depth, denoted as H. In this specific project, the excavation depth was established at 3.5 meters. The correlation between excavation depth and wall deflection underscores the critical relationship that leads to allowable lateral displacement of wall, ensuring the structural integrity and safety of the excavation site are maintained under operational conditions. In this study the maximum allowable horizontal deflection was calculated based on empirical equation 2.11 as is

expressed bellow (Moormann, 2004)

$$\delta_h = 2.5\% \cdot H \tag{2.11}$$

2.10.5 Limit state approach

The performance criteria for retaining structures and soil materials are encapsulated mainly within two distinct limit states approaches: the Serviceability Limit State (SLS), which emphasizes operational conditions of structure and structure's support components.
It is critical to check condition below for SLS design where E_k is characteristic of action effect (e.g bending moment) and C_k is for capacity or allowable limit (Orr & Breysse, 2008).

$$E_k \leq C_k \tag{2.12}$$

The Ultimate Limit State (ULS), which addresses the potential for soil failure mechanisms around structures, including sliding, rotation and of structural failure. The inherent variability in soil presents a considerable challenge for geotechnical designers in accurately predicting ground and structural performance to withstand potential failures. In ULS design same condition (equation above (2.12)) should be checked but with considering design values for E_d (ultimate worst case of action effect) and R_d(ultimate resistance).

$$E_d \leq R_d \tag{2.13}$$

In ULS design factoring material resistance or Input Factoring is a common method utilized when the dataset from sampling is inadequate. Broadly speaking, this approach involves adjusting material properties, such as applying a factor of 1.5 to undrained shear strength (deterministic value), thereby assuming the shear strength of the soil (R_d) in contact with the wall is reduced by 1.5 times(Andrew, 2012). This conservative estimate provided by Eurocode 7 ensures that, even in extreme hazard events, the retaining wall remains stable despite the diminished soil shear strength. Particularly for retaining walls, input factoring is deemed more suitable as it accounts for reduced soil strength, potentially leading to a less stable structure, nonetheless, offering a more accurate assessment for ULS conditions compared to output-factored parameters. Conversely, Output Factoring concentrates on load adjustments. In this strategy, designers amplify the load, for instance on an anchor, by a certain factor and then assess whether the design meets ULS requirements or requires reevaluation (Lees, 2016).

2.10.6 Factor of safety for geotechnical failure

The stability of soil surrounding the excavation is crucial to be assessed. The potential geotechnical failure can be assessed by analyzing factor of safety. The factor of safety can be estimated by utilizing c/phi reduction method (equation 2.14). This method applied in In PLAXIS 2D to reduces strength parameters such as the clay's cohesion(c) and friction angle (ϕ) iteratively in order to estimate different factor of safety (Brinkgreve et al., 2016). Required factor of safety can depends on regulations and the sensitivity of the project. Table 2.6 present some failure modes and

foundation type correspond to their range of factor of safety.

$$\sum Msf = \frac{tan\varphi'_{input}}{tan\varphi'_{reduced}} = \frac{c'_{input}}{c'_{reduced}} \tag{2.14}$$

Table 2.6: Common factor of safety (FS) used in foundation design (Bowles 1997 and O'Brien 2012).

Failure mode	*Foundation type*	*FS*
Shearing	Earthworks (dams, fills, etc.)	1.2–1.6
	Retaining structures (walls)	1.5–2
	Sheet-piling cofferdams	1.2–1.6
	Temporary braced excavations	1.2–1.5
	Spread footings	2–3
	Mat foundations	1.7–2.5
	Footings in uplift	1.7–2.5
Seepage	Uplift, heaving	1.5–2.5
	Piping	3–5
Shaft resistance	Deep foundations	1.5–2.5
End bearing	Deep foundations	2–3.5

3
Method

This section is dedicated to comprehensive methodology applied to investigate defined objectives of the study. Moreover, to integrate theoretical model in FE and empirical data to analyze the robustness of design by different performance criteria. The methodology used in this thesis is outlined in figure 3.1.

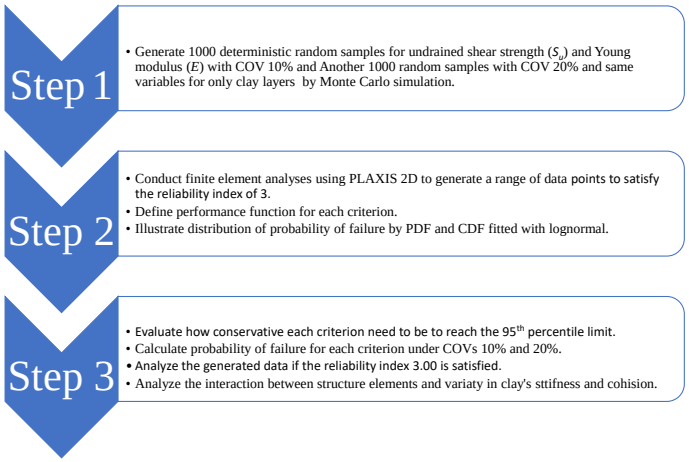

Figure 3.1: Overview of used methodology in three steps.

3.1 Case Study

Project Brf Sydney is 127 apartments which is located in dens and urban area Masthuggskajen in Gothenburg, Sweden(Figure 3.3). Excavation in urban area has its own challenges such as soil movement and wall deflection during excavation. Project area is around 3600 square meter which is surrounded by relatively large buildings. The retaining structure in the Sydney project decided to be sheet pile wall installed in the ground by the length of 12 m. The wall's profile was AU14 with the steel quality of S355. The sheet pile wall was supported laterally by waler at the level of +1.00 m with the profile of HEB450 and steel quality of S355 attached to 13.5-meter-long strut which was fixed in the concrete slab. The concrete slab designed to have a thickness of 0.2m and waler beam supported by strut (see figure 3.2) and step-wise excavation for temporary situation was selected for design. In

the bottom placed concrete slab. For site investigation cone penetration test was conducted.

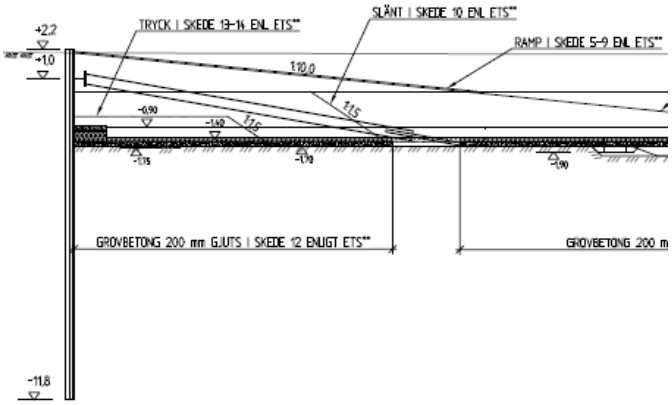

Figure 3.2: The cross section of actual retaining structure used in Sydney project included concrete slab at the bottom of excavation.

The geological characterization of the site is mainly soft clay with 2 meters thick granular fill material near the surface level. The undrained shear strength measured in situ by cone penetration test CPT, and it assumed to increase incrementally through the depth. The clay's undrained shear strength in range of 10 kPa to 70 kPa covered up to 100 depths. Undrained shear strength set to follow trend of 17 kPa by increasing 1.3 kPa incrementally with depth. The measurement of water content in site investigation shows that the water content in clay varies from 60% to 75%.

Figure 3.3: Overview of the Sydney project and its location in Gothenburg-Sweden.

3.2 Monte Carlo Simulation in PLAXIS 2D

The Monte Carlo simulation was employed to generate multivariate representations of the undrained shear strength and stiffness of clay across all clay layers. This process involved conducting the simulation 1000 times with COV of 10% and another 1000 times for a COV of 20% reflecting real world soil variability, utilizing fully automated PLAXIS 2D by Python scripts. The collective 2000 samples underwent data analysis to identify any instances of system failure. The MCS procedure explained as follows:

Generate random variables: The COV values (either 10% or 20%) were applied to the predefined mean undrained shear strength value to derive the standard deviation parameter for the random operator code in Python. The undrained shear strength (Su) was generated using a random normal variate operator in Python based on the given site characterization data for the specified variables, applicable only to the clay layers. For the clay layers, the Young's modulus (E) was calculated using the same generated value for each undrained shear strength and then multiplied by 250 kN/m^2.

FE samples: A total of 2000 random deterministic Finite Element (FE) simulations were generated to model the undrained behavior with Mohr-coulomb soil model.

Data extraction via Python: Python scripts were employed to extract critical parameters such as the factor of safety (through c/phi reduction), maximum bending moment, maximum wall deflection in the x-direction, maximum waler force, geotechnical factor of safety and combined cases. The datasets, encompassing both Serviceability Limit State (SLS) without traffic load and with line load behind the sheet pile wall, was extracted for each simulation.

Monitoring for negative values: Throughout the sample generation process, careful monitoring ensured that no negative values were produced for undrained shear strength and soil Young's modulus. However, the negative value for incremental values for undrained shear strength and Young's modulus were permitted.
Distribution analysis: The resultant data were assumed to follow a lognormal distribution, with analyses conducted to map out both the probability density function and the cumulative density function (K.-K. Phoon & J. Ching, 2015).

3.3 Numerical Analysis in PLAXIS 2D

In this section the numerical analysis used, in PLAXIS 2D for generating stochastic datapoints will be explained in detail.

3.3.1 Model geometry

The geometry of the finite element model which is one of the key features of the design process. As illustrated in figure 3.4, the model is a square shape (+2, 80) (80, -80) and the retaining wall is placed 50 meters along the x-axis, with a depth of -9.8 meters. Skanska Teknik determined the excavation depth to reach -1.55 meters, spanning an excavation length of 30 meters. It is important to note that the dry crust layer extends from +2 meters to -0.8 meters, whereas the retaining wall begins 20 cm above the surface level (+2.2). additionally, last clay layer did not divided since the impact of clay 6 on the overall results was neglectable.

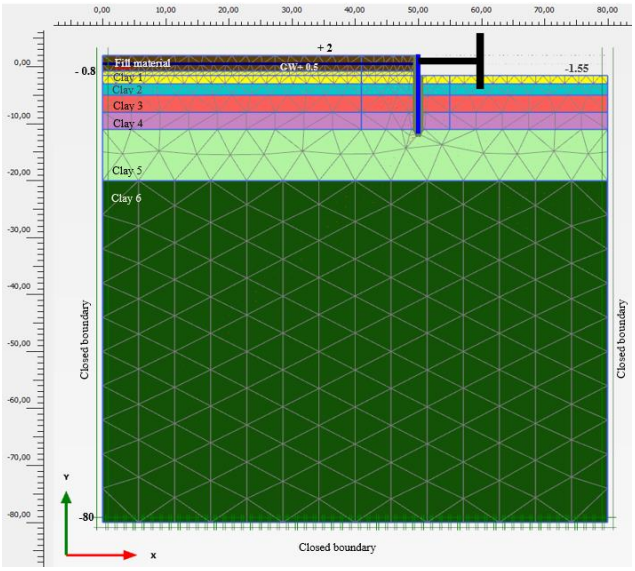

Figure 3.4: Geometry of the PLAXIS 2D model.

3.3.2 Soil model input

The constitutive soil model for this study is assigned to be Mohr-Coulomb. The drainage type for the filling material was designated as drained, whereas for all clay layers, it was set to be the undrained type ('B'). The rationale behind selecting type ('B') largely comes from the study's focus on the undrained behavior rather than drained shear strength, with the intention to mitigate the risk of overestimating undrained shear strength, a known limitation of type ('A'). However, employing method ('B') introduces a potential drawback: a higher likelihood of error in estimating pore water pressure, which poses challenges for projects that incorporate consolidation phases in their construction stages.
The soil composition comprised six distinct clay layers, with a granular layer positioned at the top of the clay strata. As previously mentioned, a random normal variant was utilized to generate a spectrum of undrained shear strengths, considering two different coefficients of variation (COV) of 10% and 20%. It's important to note that the soil stiffness (Young's modulus) across all clay layers was influenced by the variation in cohesion within each layer. Moreover, the increments in cohesion and soil stiffness were computed using the equation shown below. Tables 3.1 to 3.6 indicates that only the first and last clay layers remained consistent as original design, while clay layers 2, 3, 4, and 5 exhibited variations in their E_{inc} and C_{inc}. According to equation 3.1, negative values for E_{inc} and C_{inc} were allowed in each realization.

$$\frac{s_{u_{n+1}} - s_{u_n}}{Thickness\ of\ the\ clay\ layer} \tag{3.1}$$

Where s_{u_n} is presenting the stiffness of clay layers corresponding to their position shown by sub-index n. The entire process of generating random undrained shear strengths for the clay layers and their Young's modulus was accurately monitored to

ensure that negative values were not produced, adhering to the natural occurrence of cohesion and soil stiffness as positive values.

Finally, the soil interface was modeled with same soil model (MC) with Interface reduction factor of 0.5 (Damians et al., 2015). It can be mentioned that the choice of an interface reduction factor of 0.5 in this study was based on its common use as a moderate value, neither overly conservative nor overly optimistic.

Here's how you can create individual tables for each clay layer, ensuring each table is properly formatted and placed on a new page if necessary. I will split the provided table into individual tables for each clay layer.

Table 3.1: Soil properties for fill Material

Parameters	Symbol	Fill material	Unit
Type of behaviour		Drained	
Dry weight/wet weight		18/20	kN/m^3
Undrained shear strength	$S_{u,ref}$	1	kN/m^2
Depth-dependent undrained shear strength	S_{inc}	0	
Friction angle	ϕ	36°	
Young's modulus	$E_{3.1}$	9000	kN/m^2
Depth-dependency Young's modulus	E_{inc}	0	
Earth pressure coefficient	K0 determination	Automatic	
Interface	R_{inter}	0.50	
Soil layer thickness		1.2	m

Table 3.2: Soil properties for first clay layer.

Parameters	Symbol	Clay 1	Unit
Type of behaviour		Undrained (B)	
Dry weight/wet weight		15.50/15.50	kN/m^3
Undrained shear strength	$S_{u,ref}$	17.5	kN/m^2
Depth-dependent undrained shear strength	S_{inc}	1.3	
Friction angle	ϕ	0 °	
Young's modulus	E_{ref}	250 $\cdot S_{u,ref}$	kN/m^2
Depth-dependency Young's modulus	E_{inc}	200	kN/m^2/m
Earth pressure coefficient	K0 determination	Automatic	
Interface	R_{inter}	0.50	
Soil layer thickness		2.2	m

Table 3.3: Soil properties for second clay layer.

Parameters	Symbol	Clay 2	Unit
Type of behaviour		Undrained (B)	
Dry weight/wet weight		16.50/16.50	kN/m^3
Undrained shear strength	$S_{u,ref}$	17.5	kN/m^2
Depth-dependent undrained shear strength	S_{inc}	Equation 3.1	
Friction angle	ϕ	0 °	
Young's modulus	E_{ref}	250 $\cdot S_{u,ref}$	kN/m^2
Depth-dependency Young's modulus	E_{inc}	Equation 3.1	kN/m^2/m
Earth pressure coefficient	K0 determination	Automatic	
Interface	R_{inter}	0.50	
Soil layer thickness		2	m

Table 3.4: Soil properties for third clay layer.

Parameters	Symbol	Clay 3	Unit
Type of behaviour		Undrained (B)	
Dry weight/wet weight		16.50/16.50	kN/m^3
Undrained shear strength	$S_{u,ref}$	19.1	kN/m^2
Depth-dependent undrained shear strength	S_{inc}	Equation 3.1	
Friction angle	ϕ	0 °	
Young's modulus	E_{ref}	250 $\cdot S_{u,ref}$	kN/m^2
Depth-dependency Young's modulus	E_{inc}	Equation 3.1	kN/m^2/m
Earth pressure coefficient	K0 determination	Automatic	
Interface	R_{inter}	0.50	
Soil layer thickness		3	m

Table 3.5: Soil properties for fourth clay layer.

Parameters	Symbol	Clay 4	Unit
Type of behaviour		Undrained (B)	
Dry weight/wet weight		16.50/16.50	kN/m^3
Undrained shear strength	$S_{u,ref}$	24.8	kN/m^2
Depth-dependent undrained shear strength	S_{inc}	Equation 3.1	
Friction angle	ϕ	0 °	
Young's modulus	E_{ref}	250 $\cdot S_{u,ref}$	kN/m^2
Depth-dependency Young's modulus	E_{inc}	Equation 3.1	kN/m^2/m
Earth pressure coefficient	K0 determination	Automatic	
Interface	R_{inter}	0.50	
Soil layer thickness		3	m

Table 3.6: Soil properties for fifth clay layer.

Parameters	Symbol	Clay 5	Unit
Type of behaviour		Undrained (B)	
Dry weight/wet weight		17.50/17.50	kN/m^3
Undrained shear strength	$S_{u,ref}$	26.8	kN/m^2
Depth-dependent undrained shear strength	S_{inc}	Equation 3.1	
Friction angle	ϕ	0 °	
Young's modulus	E_{ref}	250 $\cdot S_{u,ref}$	kN/m^2
Depth-dependency Young's modulus	E_{inc}	Equation 3.1	kN/m^2/m
Earth pressure coefficient	K0 determination	Automatic	
Interface	R_{inter}	0.50	
Soil layer thickness		9	m

3.3.3 Properties of Sheet pile wall

The input values corresponding to sheet pile wall provided in table 3.7. Furthermore, the material type was defined as exhibiting elastic-plastic behavior, with isotropic geometry characteristics attributed to the plate. The technical specifications of the AU14 steel sheet pile wall is detailed in table 3.8. This documentation includes a variety of values for a one-meter plate segment, providing a comprehensive overview of the steel element's properties.

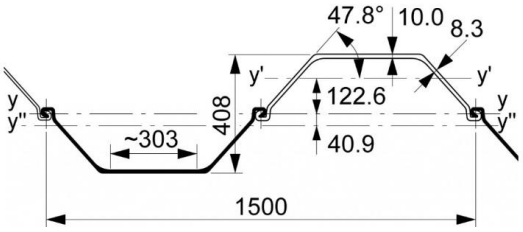

Figure 3.5: Section of AU 14 U-shape pile used in the project (ArcelorMittal, 2024)

Table 3.7: Properties of wall profile AU14.

Sectional area [cm^2]	Mass per meter [kg/m]	Moment of inertia [cm^4]	Elastic section modulus [cm^3]
132.3	103.8	28710	1410

Table 3.8: Properties for sheet pile wall AU14.

Parameter	Symbol	Value	Unit
Young's modulus	E	210	GPa
Axial stiffness	EA	2778300	kN/m
Bending stiffness	EI	60228	kNm^2/m
Poisson's ratio	ν	0	-
y' (plain strain assumption)	d	0.51	m

3.4 Structure model input

In this study the selected wall AU14 has a bending moment capacity which is calculated as follows:

$$M_{Rd} = \ W_x \cdot f_{yc} \tag{3.2}$$

$$M_{Rd} = 1.41{\cdot}10^{-3} \cdot 355{\cdot}10^{3} = \ 500 \ kNm/m \tag{3.3}$$

Where W_x, the sectional elastic modulus related to wall material properties, is 1410 cm^3 and f_{yc} is a value that depends on the quality of steel, which in this project S355 MPa was selected. It is important to highlight that the reduction factor caused by the interlocking effect was considered to be one ($\beta_D = 1$) in this study.

3.4.1 Bending moment design values based on SK2

The original design by Skanska Teknik was adhering to Safety Class 2 (SK2- Swedish standard). The calculation of action effects on wall was conducted in accordance with "Sponthandboken" (Kullingsjö et al., 2018) or the equivalent standards set out in EN 1997-1. It is essential to highlight that the partial factors selected for the design values were based on Swedish codes, specifically, for permanent and variable unfavorable loads (A2), the partial factors were determined to be 1.1 and 1.4, respectively. Additionally, the table provided below, point to the information concerning the Eurocode's partial factors for actions and soil parameters. Table 3.9 is critical for understanding the applied safety margins and the rationale behind the chosen values for ensuring the structural integrity and stability of the sheet pile-supported excavation under various loading conditions.

Table 3.9: Summary of partial factors on effects of actions.

Action		Symbol	Set	
			A1	*A2*
Permanent	Unfavourable	γ_G	1,35	1,0
	Favourable		1,0	1,0
Variable	Unfavourable	γ_Q	1,5	1,3
	Favourable		0	0

In the original design process by Skanska, it was crucial to incorporate partial factors on the effect of action loads (Ed) concerning to design bending moment value and design anchor load value. These factors were applied since designed was performed by FEM, utilizing characteristic values, and utilizing unfavorable loads resulting from surface traffic load. The design values for the moment and fixed anchor force were derived using equations outlined in equations 3.4 and 3.5 (Kullingsjö et al., 2018, p. 35).

$$M_{design} = M_{DA3,1} \cdot \gamma_d \cdot 1.10 + (M_{DA3,2} - M_{DA3,1}) \cdot \gamma_d \cdot 1.4 \tag{3.4}$$

$$S_{design} = S_{DA3,1} \cdot \gamma_d \cdot 1.10 + (S_{DA3,2} - S_{DA3,1}) \cdot \gamma_d \cdot 1.4 \tag{3.5}$$

Where $M_{DA3,1}$ and $S_{DA3,1}$ are the maximum bending moment and anchor force respectively without unfavorable load, and the maximum values considering traffic load are denoted as $M_{DA3,2}$ and $S_{DA3,2}$. Moreover, γ_d is calculated by $\frac{1}{1.1} = 0.91$.

3.4.2 Waler/ strut

In the PLAXIS 2D, a fixed-end anchor (waler) positioned at a level of +1.00 was modeled to exhibit elasto-plastic behavior. This modeling choice was reflective of the anchor's real-world connection to struts extending 13.5 meters long which should be considered in the calculation of waler's axial stiffness. This means that, to accurately calculate the anchor's real properties, the total axial stiffness of the HEB450 -S355 beam was divided by 13.5m. The specific parameters of the fixed-end anchor are detailed in table 3.10.
In the primary design, the highest allowable shear capacity of the waling beam was determined through the application of a specific equation (Equation 3.6). However, it should be noted that the buckling effect was not considered in the calculation of the maximum allowable load on the waler (Kullingsjö et al., 2018).

$$N_{Rd} = A_w \cdot f_{yc} \tag{3.6}$$

Table 3.10: Properties of waler HEB450

Parameter	Symbol	Value	Unit
Young's modulus	E	210	GPa
Axial stiffness	EA	339.1E3	[kN]
Length of spacing	L_{spacing}	8	[m]

Where A_w is the beam's cross-sectional area and f_{yc} is a value that depends on the quality of steel, which in this project is set to be S355 MPa. N_{Rd} is calculated to be $0.0218 \cdot 355000 = \frac{7739.8}{8} = 967.3$ kN.

3.4.3 Mesh

The finite element method was employed to generate a mesh that accurately configures the model's geometry and all relevant details. Through meshing, the geometry is segmented into finite elements, facilitating more precise calculations. Surrounding the sheet pile wall, a reinforced mesh was implemented to meticulously capture details around the wall's toe. Medium, fine, and very fine meshes were evaluated, however for this project, a 15-node element with a fine mesh (0.03 with 1553 – 12800 elements) was adopted for all simulations (mesh sensitivity can be seen in appendix A). The mesh is showed in figure 3.6, offering a visual representation of the modeled geometry and the refined approach to meshing within the study.

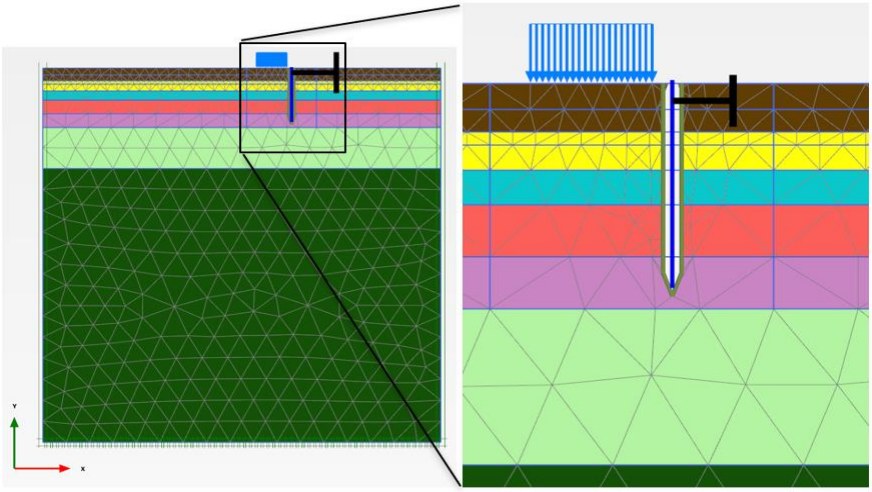

Figure 3.6: Generated fine mesh and reinforced mesh around the wall (right side)

3.4.4 Construction sequence

For simulating the construction project across multiple phases to thoroughly assess the soil and structure behavior, a 12-meter sheet pile wall was installed with the

presumption that its installation would not disturb the underlying clay layers. A groundwater level of +0.5m was designated and initially, the lateral effective stress (K_0) was applied, setting its value to 1.00, to simulate the in-situ stress conditions accurately.
In the domain of construction, projects are often segmented into various phases. In this study, analysis was split into two conditions: the first four phases simulate the Service Limit State (SLS) employing predefined characteristic values, while in the second condition, phases five to seven were dedicated to incorporating a surcharge load behind the wall followed by stability analysis. Given that the undrained type ('B') was selected for this study, no consolidation phases were accepted. Finally, the pore water pressure calculation was consistently set to the phreatic level throughout all construction phases.
Detailed construction phases are as follows:

Initial Phase:

The K_0 procedure was adopted without activating any line load.

Phase One [Sheet Pile Wall Installation]:

The retaining structure, along with its interface elements, was activated.

Phase Two [Excavation to +0.5m]:

The objective was primarily to remove the soil adjacent to the wall. Both loading and calculation types were set to plastic and staged construction for this and subsequent phases.

Phase Three [Fixed-End Anchor Installation]:

Installing a fixed-end anchor at the level of +1m.

Phase Four [Excavation to -1.55m]:

Post-activation of the fixed-end anchor, excavation of the final layer commenced to achieve a total depth of 3.5 meters.

Phase Five [Traffic Load]:

A line load was applied over a 6-meter span, finishing 1 meter before the wall's edge, with a traffic load intensity set at -20kPa.

Phase Six [Factor of Safety (FoS) Analysis]:

Shear strength reduction was employed to calculate the global safety factor, revealing the geotechnical failure post-line load application. An incremental multiplier with a maximum of 120 steps and 60 iterations was used.

Phase Seven [FoS Analysis for Phase 4]:

The potential for ground failure, prior to traffic load activation, was analyzed using a similar strength reduction method, focusing on geotechnical failure with an incremental multiplier maxing out at 100 steps.
This comprehensive approach enables a nuanced understanding of the geotechnical performance of the soil throughout the construction phases, ensuring the design's reliability and safety.

3.5 Performance function

For being able to perform reliability-based design, the limit state or performance function should be defined. These functions are involved in capturing the performance of the sheet pile wall and waler, as well as the soil behavior, specifically during Phase 4 (excavation to -1.55m) and Phase 5 (activation of the traffic load). The performance of the system was evaluated by defining a criterion such as a factor of safety less than 1.5 indicating a high risk for geotechnical failure, a maximum bending moment exceeding the allowable limit signifying structural failure, checking the performance of lateral support (waler/strut), and even the maximum deflection of the wall (LOW, 2018). Following all simulations, those that did not meet the performance criteria were identified and utilized for estimating the probability of failure using functions below.

For evaluating the performance of retaining structures, the limit state function for maximum bending moment was expressed as:

$$g_M(X) = M_{\text{Rd(AU14)}} - M_{\text{design}}$$
$$g_M(X) \leq 0 \quad \text{Failure}$$
$$g_M(X) > 0 \quad \text{Not failure}$$

Where $M_{\text{Rd(AU14)}}$ is the wall's permissible bending moment and M_{design} is the maximum bending moment calculated by equation 3.4 at phase 5.
In addition, for the waler, the performance function was expressed as:

$$g_{\text{Anchor}}(X) = S_{\text{Rd(HEB450)}} - S_{\text{design}}$$
$$g_{\text{Anchor}}(X) \leq 0 \quad \text{Accepted}$$
$$g_{\text{Anchor}}(X) > 0 \quad \text{Not accepted}$$

Where $S_{\text{Rd(HEB450)}}$ is the HEB 450 force capacity and S_{design} is the designed force obtained by each simulation.
Lastly, the performance function for total lateral wall deflection U_x was defined as:

$$g_{Ux}(X) = U_{x,\text{required}} - U_{x,\text{Maximum}}$$
$$g_{Ux}(X) \leq 0 \quad \text{Accepted}$$
$$g_{Ux}(X) > 0 \quad \text{Not accepted}$$

Where $U_{x,\text{required}}$ is the 9 cm allowable wall displacement and $U_{x,\text{Maximum}}$ is the maximum displacement obtained in every simulation.

The performance of the soil surrounding the wall and the factor of safety was inspected by employing the limit function, which defines the boundary between safety (indicated by positive values exceeding zero) and the unsafe zone or high risk for collapse (marked by negative values and zero). This differentiation is crucial under the varying conditions induced by COVs of 10% and 20%. The assessment of geotechnical failure encompasses:

$$g_{\text{FoS}}(X) = \text{FoS}_{\text{Generated by MCS}} - 1.5$$

$$g_{\text{FoS}}(X) \leq 0 \quad \text{High risk for collapse}$$

$$g_{\text{FoS}}(X) > 0 \quad \text{Safe}$$

Where $\text{FoS}_{\text{Generated by MCS}}$ represents the actual factor of safety in each phase for individual simulations and 1.5 is the required factor of safety based on the Swedish design code.

4

Results and discussion

4.1 Undrained Shear Strength and Stiffness

Understanding the randomness of soil's parameters in nature is crucial to picture the realistic soil's strength. In this study, different levels of uncertainties were added to the clay's cohesion and stiffness to generate a distribution of random samples for each mentioned variable. Figure 4.1shows the generated random samples for undrained shear strength for six different clay layers by considering the COV 10% in 1000 simulations followed by the statistical information of generated data for each clay layer provided in table 4.1 .

All samples (C_u 1, 2, 3, 4, 5, and 6 correspond to undrained shear strength for six clay layers (from left to right layer 1, 2, 3, ..., 6)) are lognormally distributed symmetrically around the predefined mean for each clay layer. As figure 4.1 and 4.2 shows, the x-axis displays the range of generated undrained shear strength samples in the Monte Carlo simulation and the y-axis presents the probability of occurrence in percent. Furthermore, it should be noted that there are no negative values in the entire dataset.

By considering the mean value after generating a collective 2000 simulations for both COVs 10% and 20%, the stochastic mean values are almost the same as the predefined values for each layer. However, by considering the standard deviation for each layer in COV 10% and comparing it with COV 20%, wider dispersions have appeared in COV 20%. For example, comparing the first and last layers simulation results with COV 20%, the standard deviation increased from 3.37 kPa to 5.41 kPa, while the standard deviation changed from 1.65 to 3 kPa with COV 10%. COV 20% samples indicate the increasing spread in generated samples with increasing COV values.

The tables 4.1 and 4.2 highlight a marked discrepancy between the minimum and maximum values of soil stiffness across various strata, a trend particularly notable when inspecting the Young's modulus data. Notably, there is a consistent increase in soil stiffness beyond the second clay layer, as it is predicted. Crucially, when the data with COV 20% is compared with COV 10%, the difference between the minimum and maximum stiffness values becomes more pronounced, indicating a substantial influence of the COV on the variability of the soil's mechanical properties. The substantial difference is even showed that standard deviation for COV 20% is increasing, highlighting a significant increase in variability in generated stiffness and cohesion as the COV increase. The difference in the standard deviation evidently signifies a marked increase in the range of generated soil stiffness for all clay layers.

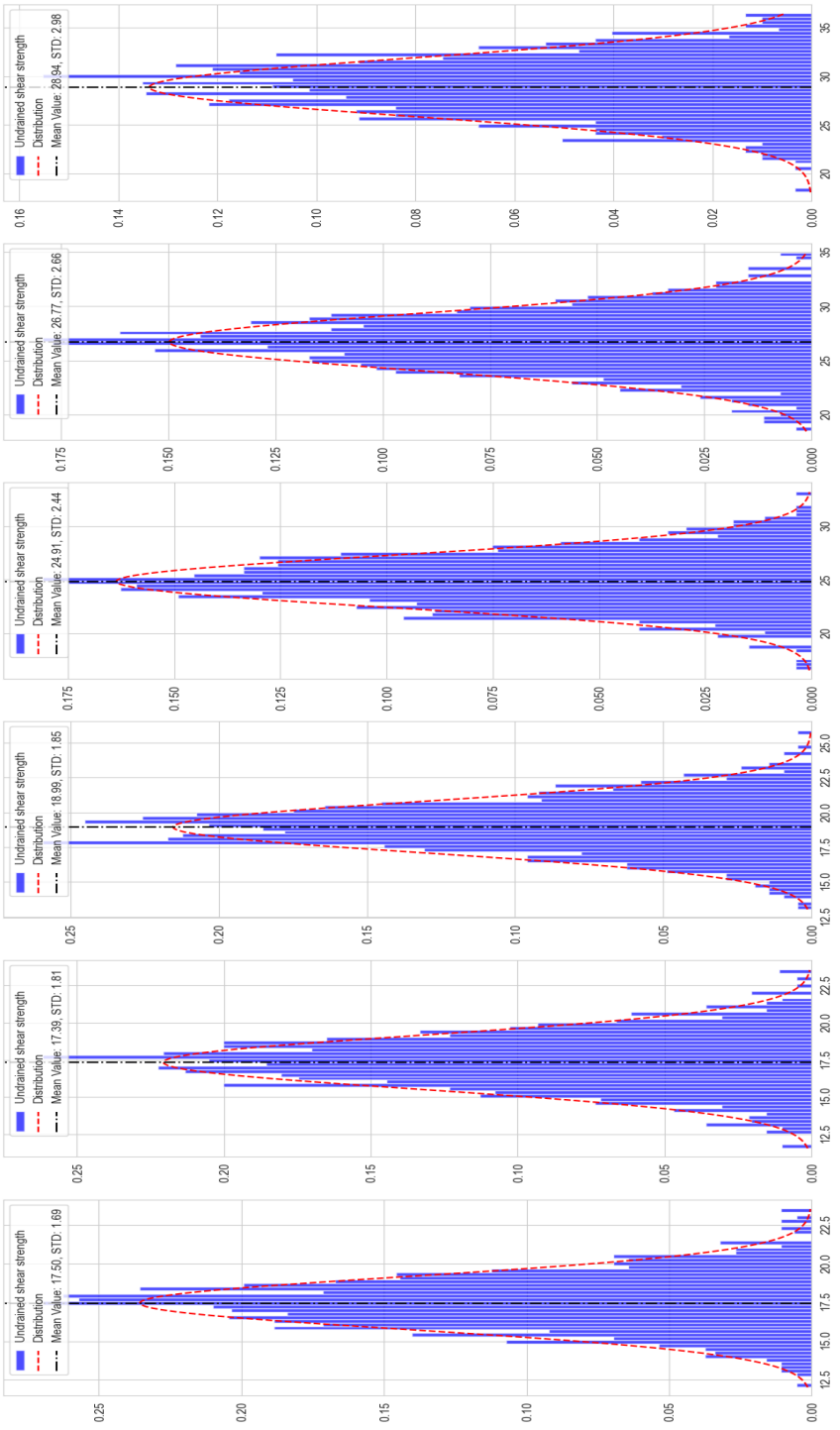

Figure 4.1: 1000 realizations generated by MCS in PLAXIS 2D under COV 10%. Samples are log-normal distributed around given cohesion value for each clay layer.

Table 4.1: Statistical information for each clay layer, extracted for undrained shear strength (Cu) and Young's modulus(E) with COV 10%.

Parameters	Mean	STD	Min	Max	Unit
Cu(clay1)	17.50	1.69	12.07	23.55	kN/m^2
E clay1	4377.7	424.3	3017.5	5887.4	kN/m^2
Cu(clay2)	17.39	1.81	11.60	21.96	kN/m^2
E clay2	4342.8	452.6	2900.2	5896.2	kN/m^2
Cu(clay3)	18.99	1.85	13.57	24.61	kN/m^2
E clay3	4745.1	459.4	3271.1	6152.8	kN/m^2
Cu(clay4)	24.91	2.44	18.42	31.64	kN/m^2
E clay4	6218.9	609.7	4150.8	8313.7	kN/m^2
Cu(clay5)	26.77	2.66	19.41	34.98	kN/m^2
E clay5	6698.5	662.7	4836.9	8745.0	kN/m^2
Cu(clay6)	28.87	2.98	18.15	36.18	kN/m^2
E clay6	7234.4	752.7	4537.8	9108.0	kN/m^2

Table 4.2: Statistical information for each clay layer, extracted for undrained shear strength (Cu) and Young's modulus(E) with COV 20%.

Parameters	Mean	STD	Min	Max	Unit
Cu(clay1)	17.61	3.40	7.28	28.48	kN/m^2
E clay1	4402.48	850.60	1820.97	7119.12	kN/m^2
Cu(clay2)	17.42	3.58	6.63	28.73	kN/m^2
E clay2	4354.69	894.54	1656.55	7182.58	kN/m^2
Cu(clay3)	19.03	3.79	5.99	28.54	kN/m^2
E clay3	4757.33	948.62	1497.76	7134.00	kN/m^2
Cu(clay4)	24.68	4.93	8.68	42.26	kN/m^2
E clay4	6170.21	1233.23	2169.96	10564.99	kN/m^2
Cu(clay5)	26.87	5.58	6.52	44.16	kN/m^2
E clay5	6717.52	1395.09	1629.42	11040.00	kN/m^2
Cu(clay6)	28.84	5.55	9.57	49.02	kN/m^2
E clay6	7209.47	1387.51	2393.03	12255.75	kN/m^2

The provided data demonstrate that the level of uncertainty significantly influences the range of generated outcomes. With a COV of 10%, the outcomes are more narrowly distributed around the predefined mean values, with a lower standard deviation for the soil's undrained shear strength and stiffness. In contrast, increasing the uncertainty to a COV of 20% results in a higher standard deviation for soil variables, generating a wider range between minimum and maximum values for each layer compared with COV 10%. A higher coefficient of variation leads to

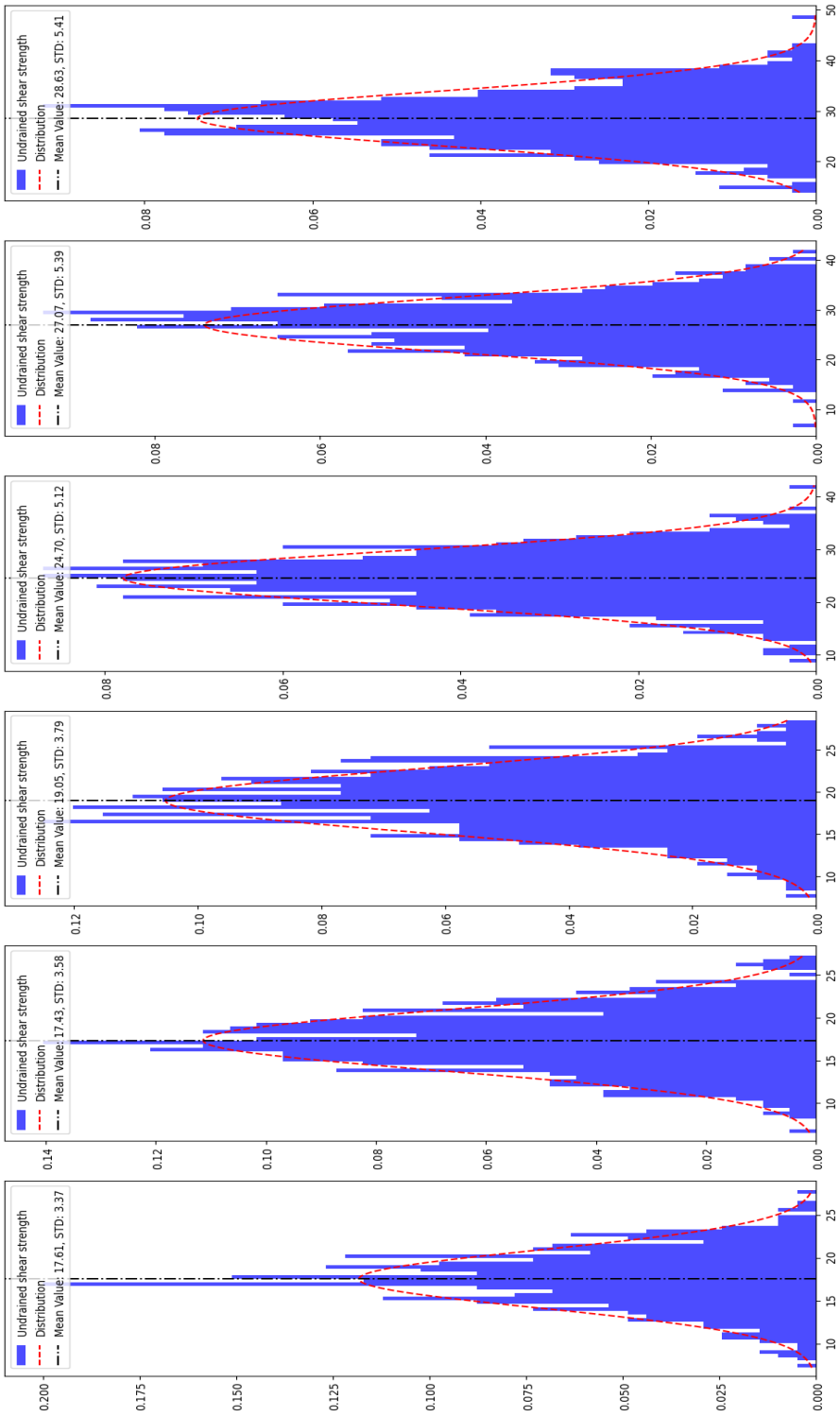

Figure 4.2: 1000 realizations generated by MCS in PLAXIS 2D under COV 20%. Samples are log-normal distributed around given cohesion value for each clay layer.

more unpredictable values for both variables. The increased variability in these two variables can highlights the greater probability of failure associated with low stiffness and cohesion in the layers near to wall's toe. Low stiffness and cohesion in critical layers can elevate the risk of unpredictable behavior of soil. The non-linear effects of higher uncertainty in soil stiffness and cohesion on the retaining structure underscore the necessity of investigating natural variability. This should be done by assessing the reliability of the design rather than merely applying partial safety factors. The overall results clearly indicate that higher levels of uncertainty lead to more expensive design due to increasing uncertainty.

4.2 Bending Moment

The structural behavior subjected to variability of soil along the length of sheet pile wall was evaluated. Graphical illustrations are reflecting the bending moment response to different undrained shear strength with different degree of uncertainties for AU14 wall in phase 4 and phase 5. All stochastic realizations compared with deterministic design which presented in each graph below. As it presented in figure 4.3 the range of max bending moment is between 105 to 186 kNm/m, which can be indicated that the result is relatively concentrated toward anchor position and end of the sheet pile wall with COV 10%. Moreover, the position of max bending moment is located in range of level -2 and -3.5 which shows the reaction of the wall near the bottom of excavation. Higher bending moment in this this section of wall can be correlated with generated weaker undrained shear strength in soils near to this level.

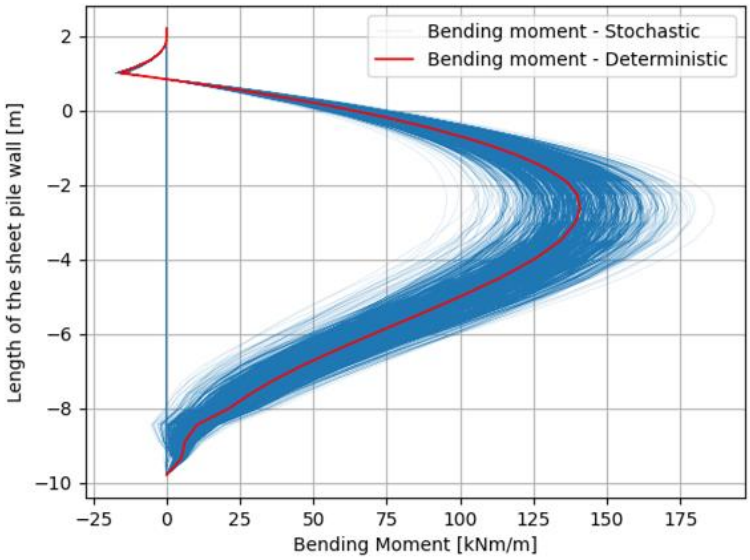

Figure 4.3: Results of 1000 realizations for bending moments (blue lines) along the 12m wall with COV 10% compared with single deterministic case (red line) at phase 4.

In contrast, by comparing the range of generated data for bending moment with COV 20%, the spreading of bending moment along the length of the wall is larger

specially toward the end of wall. As a result, the minimum and maximum bending moment cover the wider range compared to COV 10%. Figure 4.4 shows that highest bending moment along the wall start from lowest peak 70 kNm/m and reach to its highest value 218 kNm/m (105 to 186 kNm/m with COV 10more interestingly, stochastic bending moments under COV 20% have covered a much larger range especially those with negative values near the toe of the wall compared with deterministic case. Additionally, around surface level, the stochastic realizations start to differentiate and the divergence progress toward bottom of excavation, reveal the different responses of the wall to soil variability in different clay layers specially toward the end of wall.

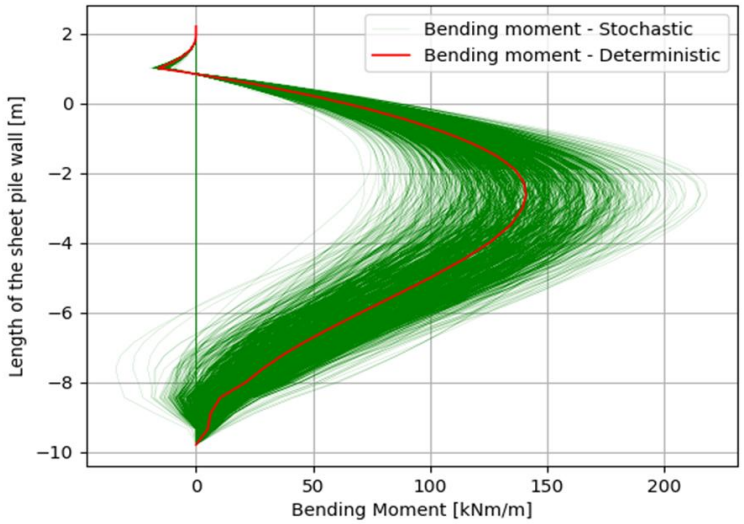

Figure 4.4: Results of 1000 realizations for bending moments (blue lines) along the 12m wall with COV 20% compared with single deterministic case (red line) at phase 4.

Subfigures 4.5 and 4.6 consider only to maximum bending moment in phase 4(excavation) and 5(activating of line load) for each simulation presented PDF with COV 10% and COV 20% respectively. The provided result of maximum bending moment in phase 4 can present that COV 10% shows highest probability of occurring maximum bending moment equal to 141.69 kNm/m which is close to maximum bending moment of deterministic design. The 95th percentile, indicated by a purple line, suggests that for a cautiously viable bending moment, the value of deterministic design should be increased by a factor of 1.18 and 1.30 with COV 10% and 20% respectively to meet the criteria of conservative design for phase 4. Additionally, it is evident that, the majority of realizations falls in the range of 96 to 186 kNm/m with COV 10% and higher range with COV 20%, from 70 to 217 kNm/m in phase 4.

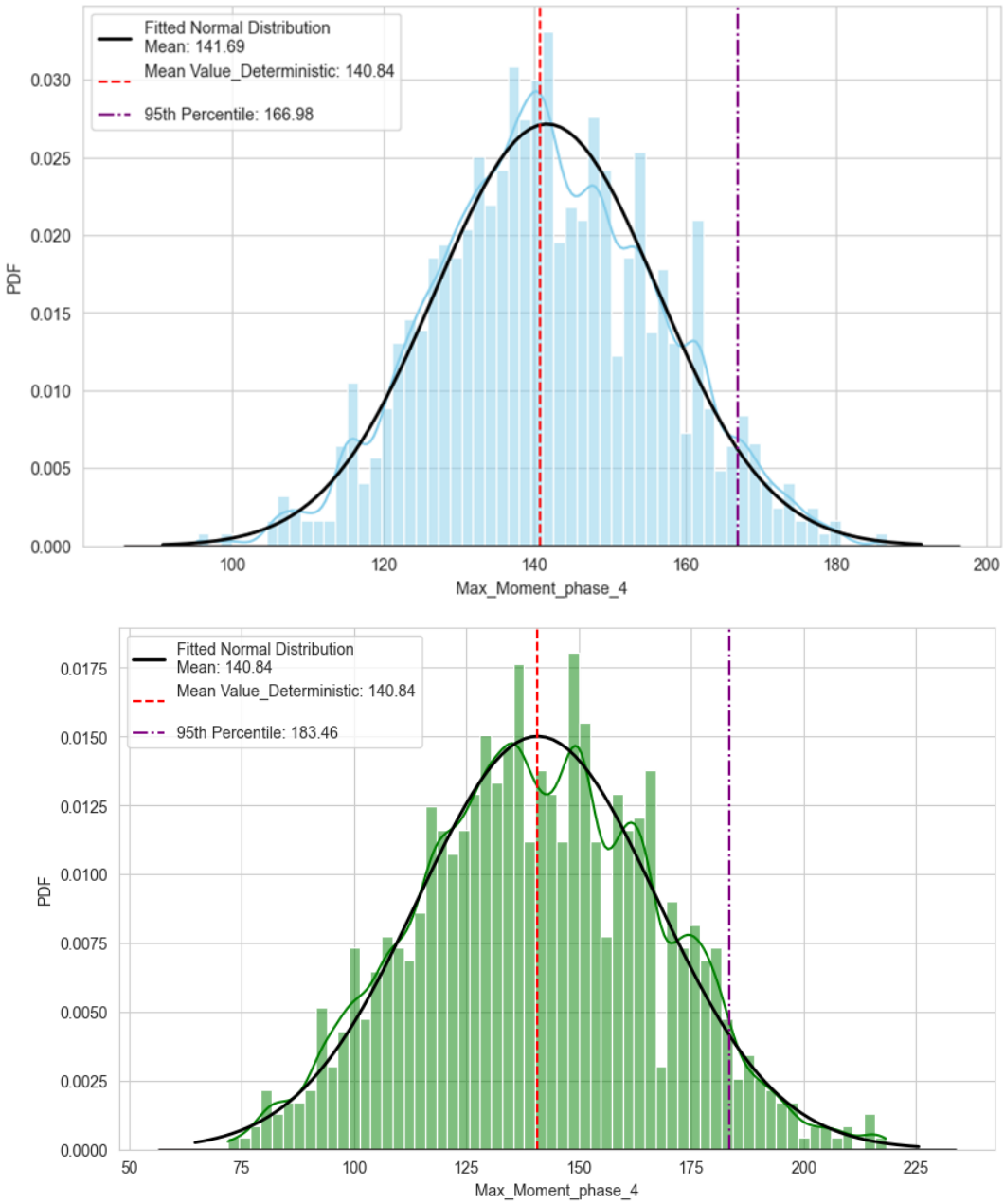

Figure 4.5: Distribution of maximum moment in phase 4 with COV 10%(blue histogram) and COV 20%(green histogram).

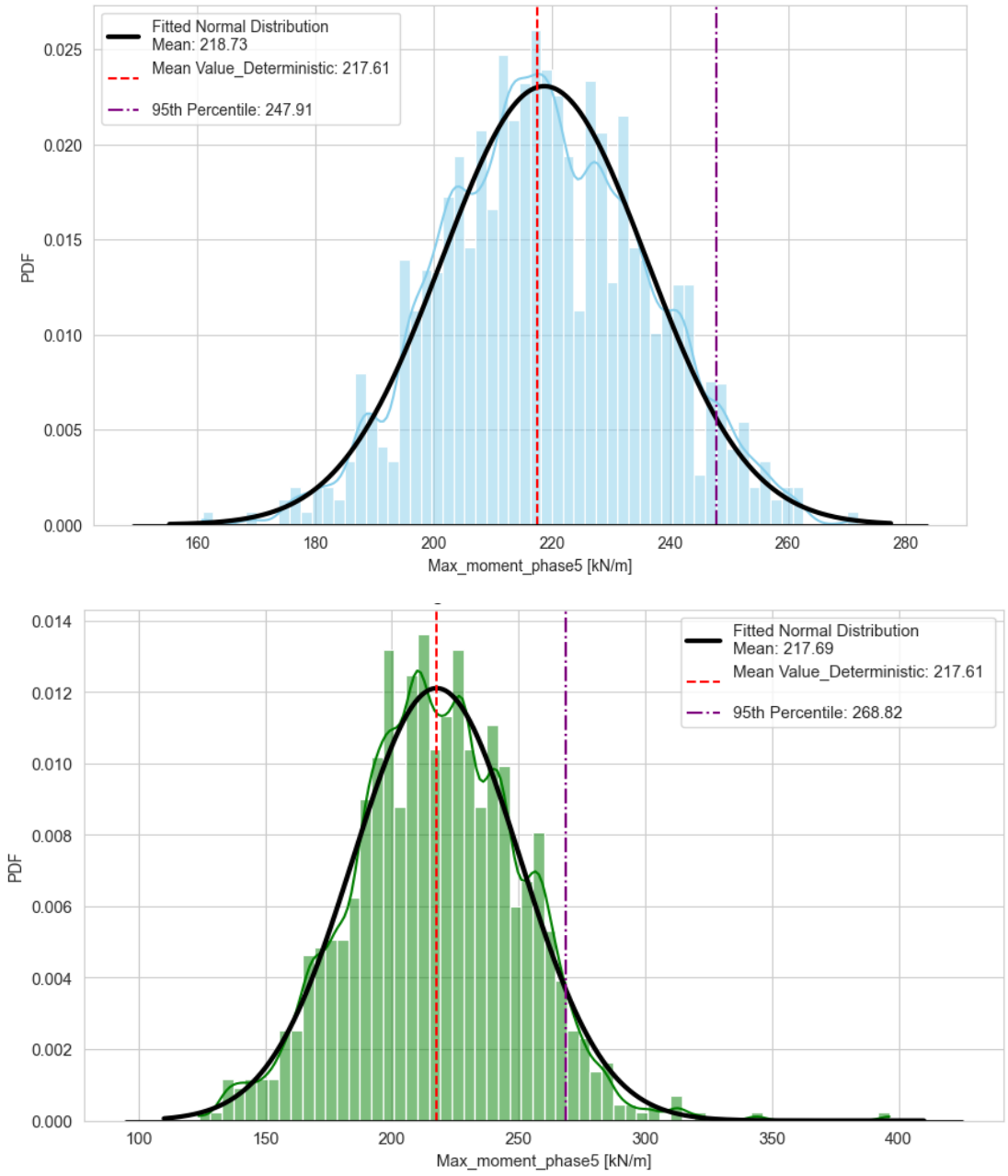

Figure 4.6: Distribution of maximum bending moment considering traffic load (phase 5) with COV 10%(blue histogram) and COV 20%(green histogram).

The presence of traffic loads in Phase 5 considerably extends the range of potential maximum bending moments. The likely maximum bending moment slightly declines from 218.73 kNm/m at COV 10% to 217.69 kNm/m at a 20% COV. Notably, the data span for the latter encompasses a more extensive range of plausible maximum bending moments, stretching from 135 to approximately 400 kNm/m, as demonstrated in Figure XX. The 95th percentile, indicated viable bending moment of 247.91 kNm/m for a COV 10% and 268.8 kNm/m for a COV 20%. These results reveal that the feasible maximum bending moments during Phase 5 have the potential to be greater than the deterministic values, with safer factors of 1.13 and 1.23

for COVs of 10% and 20%, respectively. Post-calculation analyses using equation 3.4 were conducted to assess the effects of actions load on the sheet pile wall by integrating results from Phases 4 and 5. Figure 4.7, presents the range of moments' design values under a COV of 20% spans higher and approaches to near the wall's bending moment capacity of 500 kNm/m. This proximity to the wall's capacity should be regarded as an indication of a high risk of wall failure. When considering the 95th percentile, it is notified that the deterministic moment design value be increased by a factor of 1.13 for a COV of 10% and by 1.22 for the higher COV to improve safety margins. It is noteworthy that, across the 2000 realizations collectively analyzed, the performance function for bending moments was met although the deterministic value should be shifted to more conservative side. Moreover, there was a singular observation under a COV of 20% that nearly reached the allowable limit.

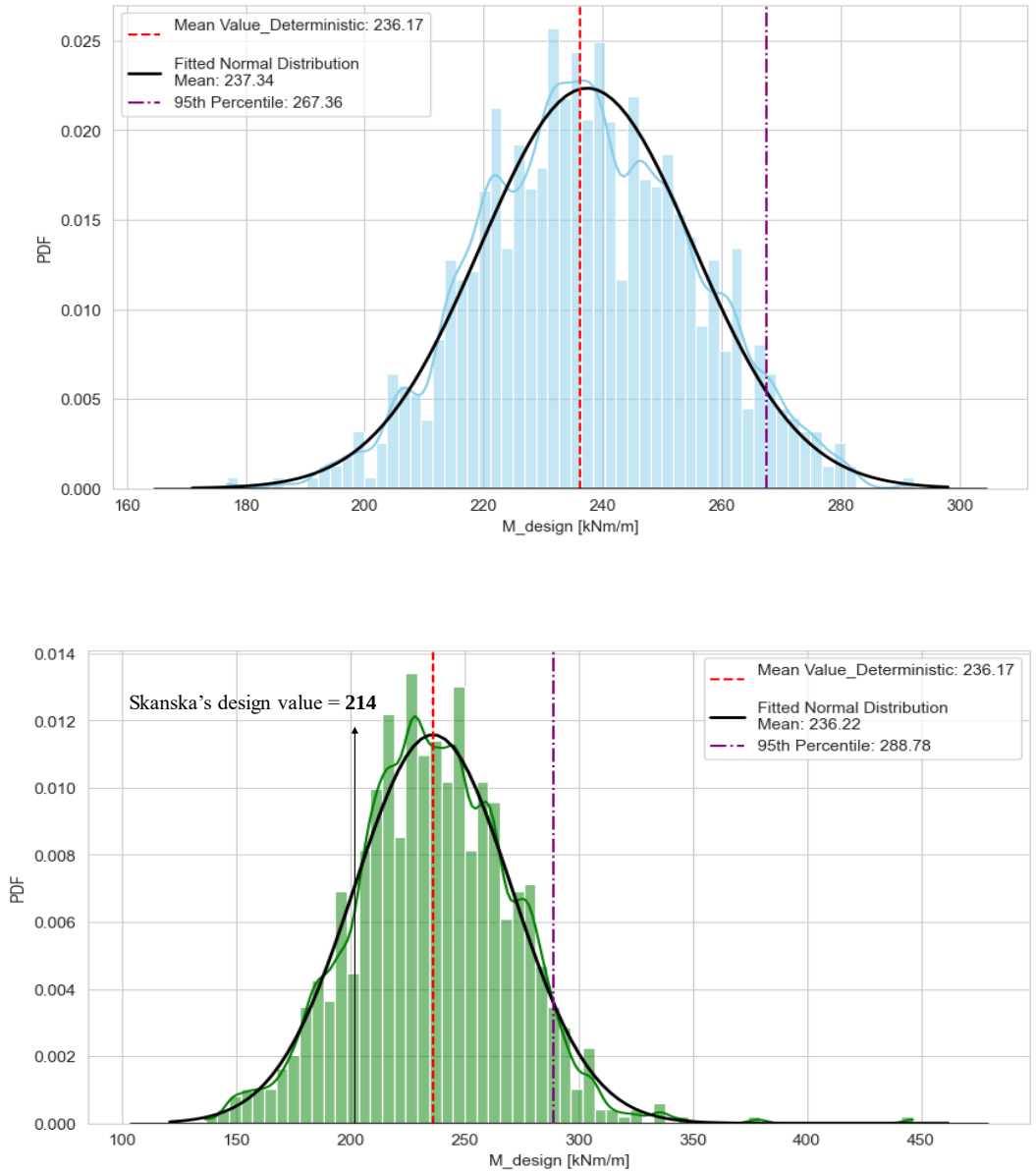

Figure 4.7: Calculated design value of bending moment in each simulation with COV 10% (blue histogram) and COV 20% (green histogram). Black arrow shows the Skanska' s design value set to be 214 kN/m.

The analysis of the bending moment along the sheet pile wall demonstrates the sensitivity of the embedded sheet pile wall to soil variability. The observations are consistent with previous studies, indicating that an increase in the coefficient of variation (COV) can lead to a decline in clay's strength-related parameters such as stiffness and cohesion. Consequently, maximum bending moment increases, highlighting the significant influence of soil variability observed in phase 4.
Additionally, in phase 5 the presence of a traffic load behind the wall exacerbates the impact of soil variability, with the combined effect of depth of each layer shifting

the maximum bending moment towards the wall's limit, approaching failure. The results indicate that the soil layers are unable to effectively mobilize the load from the surface, resulting in a larger load distribution on the wall in phase 5 compared to phase 4. The presence of traffic load significantly increases the risk of wall failure in phase 5, particularly at a COV of 20%, compared to lower COV. This response suggests that a COV of 20% generates extreme variations in stiffness and cohesion, causing potential risk for structure failure.

A single deterministic moment analysis reveals the extent to which the design value must be conservative by comparing it to the 95th percentile. The comparison of design values showed that deterministic design needs to be increased by at least a factor of 1.22 to adequately address dynamic loads, soil variability, and achieve a minimum level of conservatism to meet the reliability index of 3.00. It is notable that there is a large difference between the moment design value determined by hand calculations and the minimum level of conservative design values determined by PLAXIS 2D. Several reasons can lead to this discrepancy. In hand calculations, the material model, soil model, and wall interface effects are not considered, the range of variability in soil parameters is not examined, and the effect of wall deflection on bending moment is ignored. In contrast, numerical modeling considers all these factors, providing a more realistic picture of risk and the potential behavior of the wall within a range of outcomes. However, it should be noted that the results generated in this study were based on the Mohr-Coulomb soil model with an interface factor of 0.50, which may lead to overestimations of outcomes determined by PLAXIS 2D. There is no doubt, hand calculation offered more economical design which mostly based on assumptions that fails to capture the complex non-linearity between structure elements and soil properties while the PLAXIS include the complex interaction between structure elements and more adaptability by presenting a range of outcomes and capturing many failure modes. These evidences reveal that cheaper design can not be transparent in terms of risks and the clients should consider all mentioned details in their decisions.

4.3 Waler Force

The distribution of maximum anchor forces, adjusted for an anchor spacing of 8 meters, is depicted for both Phase 4 and Phase 5 at a COV of 10% in figure 4.8. Notably, the average anchor force for Phase 4 closely mirrors the deterministic value, with the most conservative estimate reaching -150.7 kN/m. This suggests a conservative margin factor of 1.09. A similar pattern is observed in Phase 5, where the margin of conservatism is slightly lower at 1.07. Additionally, the inclusion of traffic load appears to affect the range of axial forces on the anchor, emphasizing the necessity for a more robust design.

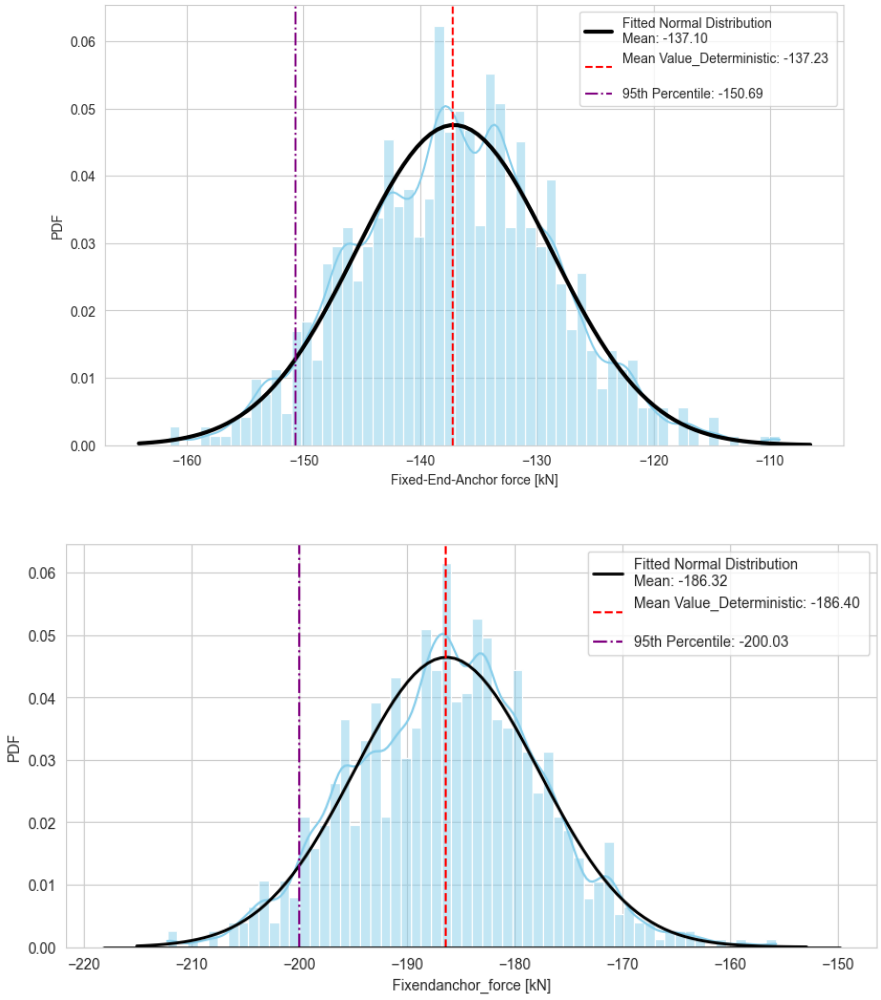

Figure 4.8: Distribution of waler (Fixed-End-Anchor) load in phase 4 and 5 with COV 10%.

Lastly, results under COV 20% presents in figure 4.9. As it shows in phase 4, stochastic and deterministic values are closely estimated to -137.2 kN however, the critical 95% value in far left shows the value of -160.8 kN which is presenting that, deterministic value is not conservative enough and it needs to be increased by a factor of 1.17.

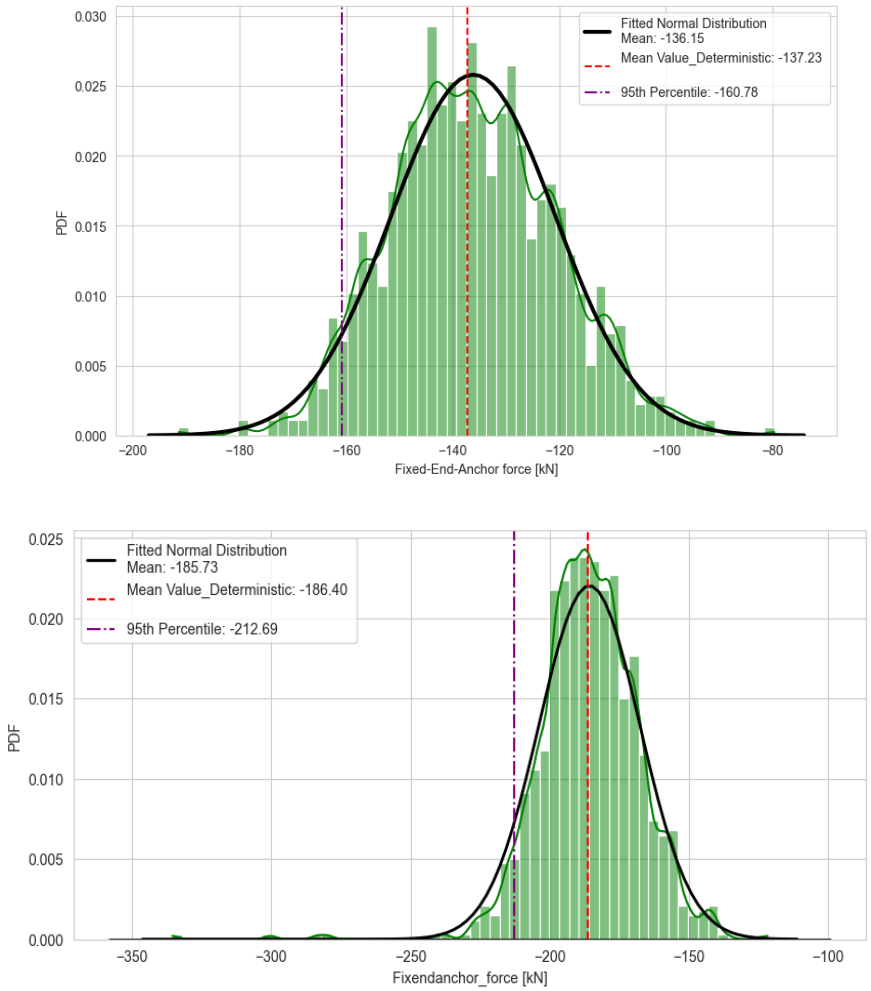

Figure 4.9: Distribution of waler(Fixed-End-Anchor) load in phase 4 and 5 with COV 20%.

The mean of stochastic and deterministic are indicating to very close value as it is reported in figure 4.10. By considering to 95th percentile, the force increased to -211.69 kN/m and it is indicating to improvement by a factor of 1.15. The design values are indicating the distribution of action effect on waler is in higher range from 135 to almost 400 kN and even the mean values for both COV 10 and 20% cases shifted to higher values and reached to -197.8 and -203.5 kN/m respectively. Inaddition, the 95% value point to value about 231 kN/m (COV20%) which is indicating that deterministic value should be increased by 1.16 to meet a cautious design. Additionally, it can be noted that there is almost 100 kN/m difference between Skanska's design value by using hand calculation and design value determined by PLAXIS 2D in phase 5.

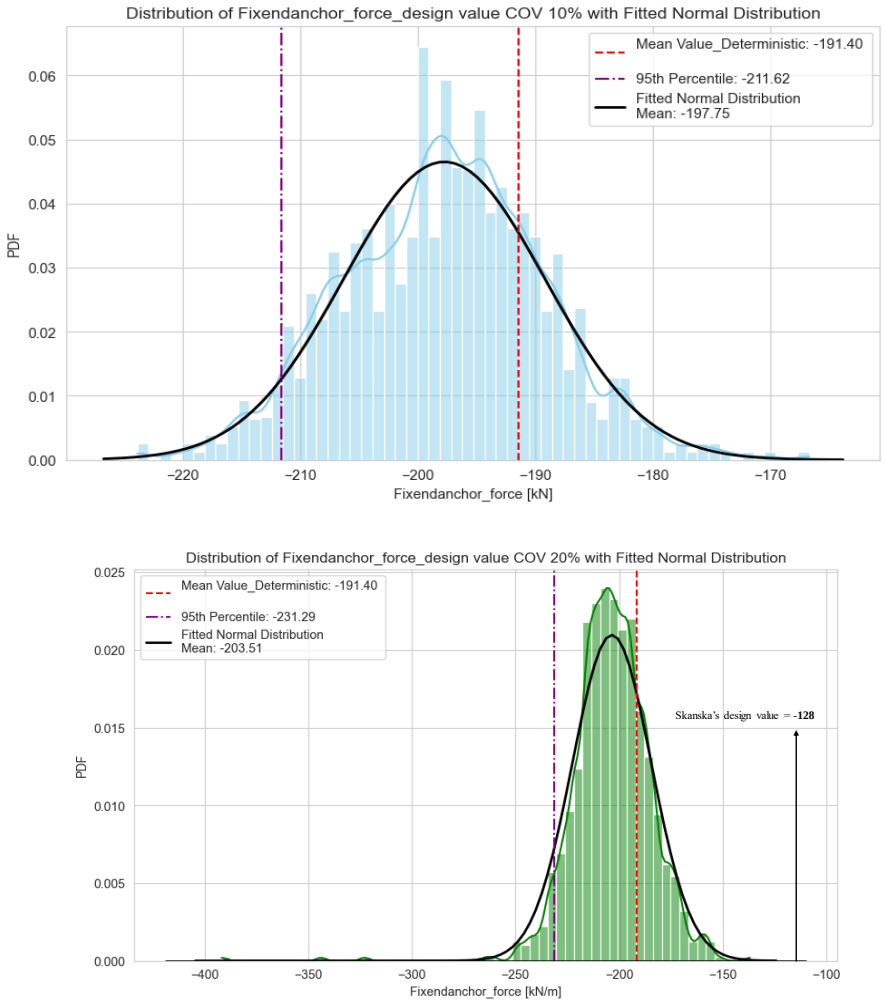

Figure 4.10: Waler's action effect (design values) under COV 10% (blue histogram) and COV 20% (green histogram). black line arrow shows the design value of 128 kN/m based on hand calculation by Skanska.

Monte Carlo Simulation results indicate a dramatic decrease in design reliability with the addition of 20% uncertainty to the soil variables, as evidenced by the doubling of the highest load on waler/ strut when the coefficient of variation increases from 10% to 20%. The combined effect of traffic load and soil variability significantly increases the risk of unpredictable events. Moreover, the deterministic design fails to adequately capture all unpredicted realizations caused by the variability in clay's cohesion and stiffness.
An investigation of 2000 simulations reveals that variability in soil stiffness and undrained shear strength has a substantial impact on the generated load and horizontal support. The maximum generated load in worst case reveal that almost half of waler's capacity was used and the deterministic value need to be increased only by 1.16 to meet the conservative limit. However, it should be noted that if buckling effects are not considered in the calculations, the force generated by the traffic load does not exceed the waler's resistance limit. This highlights the importance of using an elastic-plastic model type in numerical modeling for walers, as tradi-

tional hand calculations may not adequately account for these materials' behavior. Additionally, there is a significant discrepancy between the designed value of 128 kN/m calculated by Skanska and the minimum required design value of 229 kN/m determined by PLAXIS 2D. This discrepancy underscores how traditional hand calculation methods by assuming uniform soil properties and linear response of the soil through the depth can underestimate the potential behavior of waler. Notably, increasing loads due to uncertainty in clay's strength-related variables and the effects of non-linear response were captured by numerical models. Furthermore, meshing effect and the possibility of analyzing staged construction effects on final calculation can be other reasons why there is a large difference in the result of design values determined by PLAXIS 2D and traditional hand calculation.

4.4 Wall Deflection

The accurate prediction of wall displacement in the horizontal direction is one of the key understandings to have safe excavation. As the provided result in figure 4.11 shows, in the first scatter plot demonstrates wall deflection in horizontal direction under a COV of 10%, while the second plot illustrates deflection under a COV of 20% along the length of the sheet pile wall (y-axis). Red dotted data points deterministic results are marked with, and the black dashed line indicates the maximum allowable deflection of 0.09m. It is critical to mention that these results do not account for the influence of a concrete slab at the base of the excavation, where the deflection threshold is established at 9 cm. As it is expected, under a COV of 10%, a more constrained range of deflection is observed at the wall's toe, approximately 7 to 12 cm, which exceeds the required deflection by 3 cm. moreover, this indicates that the greatest lateral movement occurs at the base of the wall, aligning with typical behavior arising from increased moments and shear forces at the lower sections.

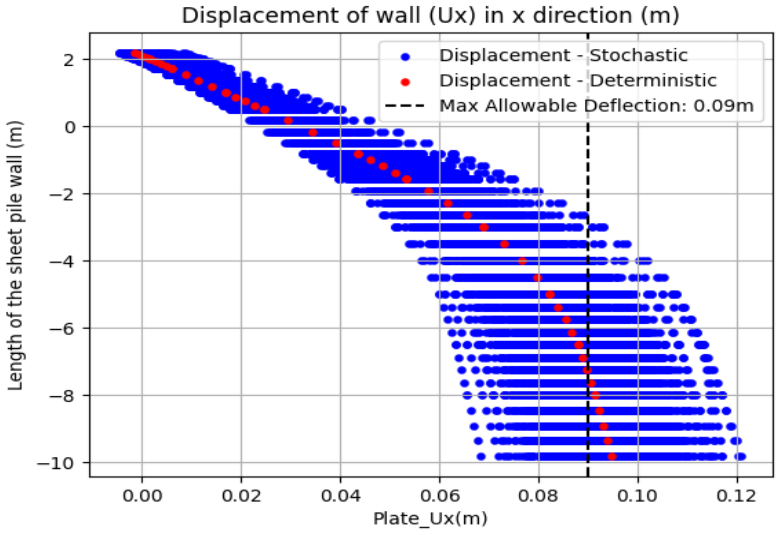

Figure 4.11: Generated deflection of sheet pile wall (Ux) in x direction under COV 10% in phase 4.

Conversely, figure 4.12 demonstrates a broader spread of displacements under a higher COV. Here, the toe of the wall exhibits increased lateral movement, with the maximum displacement reaching up to 17 cm. The wall's displacement has enhanced from it's previous maximum value of 12 cm to new peak value of 17.5 cm with the rise in coefficient of variation, equating to an almost 50% increase in maximum lateral deflection at the toe of the wall. The deterministic case nearly reaches the established limit in addition, the aggregation of stochastic outcomes signifies that wall deflections frequently exceed serviceability thresholds, highlighting the impact of soil variability, particularly at the wall's toe. The analysis of 2000 simulations reveals that a rigid sheet pile wall, reinforced by waler/strut, is prone to rotation at the toe. Notably, it is more accentuated in simulations under a COV of 20%, ranging from 5 cm to 17 cm, especially near the base.

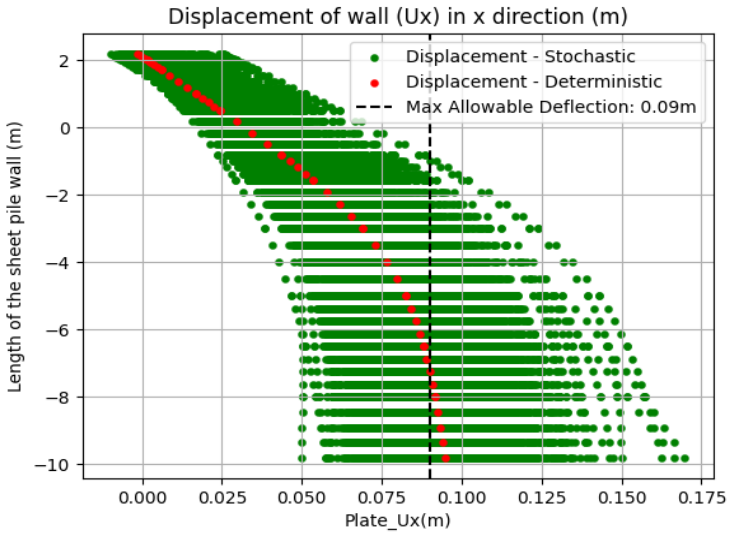

Figure 4.12: Generated deflection of sheet pile wall (Ux) in x direction under COV 20% in phase 4.

Finally, based on provided data, the probability of failure under condition of COV 10% was 54% and slightly higher at 58% for COV 20%.

The analysis reveals the significant impact of force imbalance on wall deflection, particularly near the bottom of the wall. Horizontal deflection increases noticeably with rising uncertainty in clay's variables. The performance function analysis indicates a risk of wall deflection exceeding over the defined limit, highlighting the need to reevaluate the design to manage wall deflection within acceptable bounds.
Lateral wall deflection tends to increase with greater variance (more spreading between min and max values) in cohesion and soil stiffness. Higher spreading can be attributed to the fact that decreases in clay's input properties create imbalanced forces behind and in front of the wall, potentially leading to rotation failure. The behavior of the wall in response to increasing COV suggests that reinforcement of the wall, such as the installation of a concrete slab, may be necessary to mitigate these risks. Unaddressed wall deflection could result in higher risks and challenges.

Moreover, deterministic wall deflection tend to underestimate potential wall deflection caused by soil variability, especially in clay layers 4 and 5. Underestimation of potential rotation of wall emphasizes the importance of incorporating probabilistic methods in design processes to accurately assess, mitigate and even be prepared for potential risk of rotation of wall associated with soil variability.

4.5 Factor of safety (FoS)

Assessing geotechnical failure risks due to excavation and the additional impact of traffic loads is crucial for preventing soil failure. Analyzing a range of soil performance under different conditions can be a vital indicator to assess the risk of failure by assessing geotechnical safety factor throughout all realizations. subfigurs 4.13 illustrate the generated factors of safety using the c/phi reduction method for excavation (Phase 4) represented by the green curve, and traffic load (Phase 5) indicated by the blue curve. A factor of safety threshold of 1.5 was utilized as the criterion for acceptability, with values below this threshold considered unaccepted. These stochastic results are placed alongside with the deterministic design factors of safety, which were 1.67 for Phase 4 and 1.44 for Phase 5, shown by two vertical lines. Considering the results for Phase 4 with a COV of 10%, the design exhibits a robust performance, with nearly 5% of designs falling at or slightly below the 1.5 threshold, down to 1.45. However, the effect of traffic loads on the factor of safety is significant. The CDF for Phase 5 reveals a reduction in safety caused by traffic load, with only 80% of all probable scenarios meeting the safety factor below or equal to 1.5.
With a COV of 20% , there is a noticeable shift to the left and increased variance in the results for both phases. The lower bound for Phases 4 and 5 exhibit a tendency towards lower safety factors, with the minimum safety factor moving towards more unstable values of 1.1 for Phase 4 and 1.0 for Phase 5. Conversely, the upper bound for both phases suggests a wider range, achieving safer factors of 2.2 and 1.7 respectively. Noteworthy is the 95th percentile for Phase 4, which suggests safety factors of 1.8 and 1.9 for COVs of 10% and 20%, respectively. However, for Phase 5, considering the 95th percentile, it's observed that a minority of cases marginally exceed over the 1.5 safety factor for both COVs.
Comparing the deterministic values with collective 2000 stochastic simulations reveals that the deterministic safety factors fall short of the set threshold for Phase 5, while remaining within the safe region for Phase 4. Evidently, Phase 5 has not satisfy the safety limit of 1.5 in 80% of cases (COV 10%), indicating a higher likelihood of inadequate safety compared to Phase 4 for both COV scenarios. In contrast, the probability of achieving a reliable design in Phase 4 is noticeably higher, with less than 5% of cases under COV 10% and 23% under COV 20% yielding factors of safety below the 1.5 threshold.

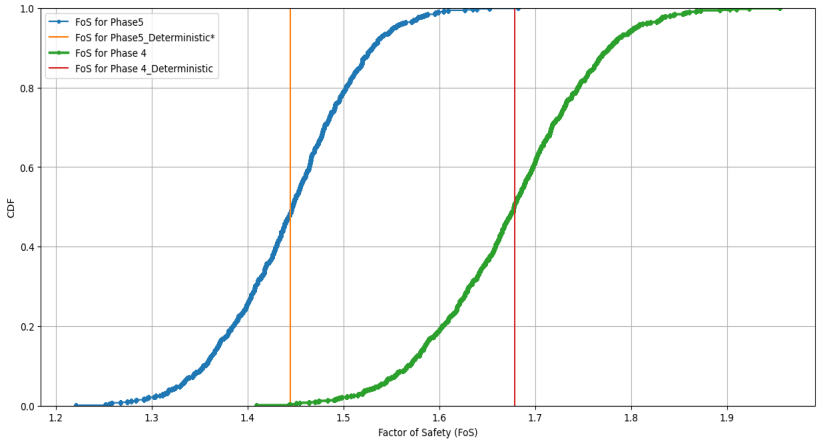

[COV 10%]

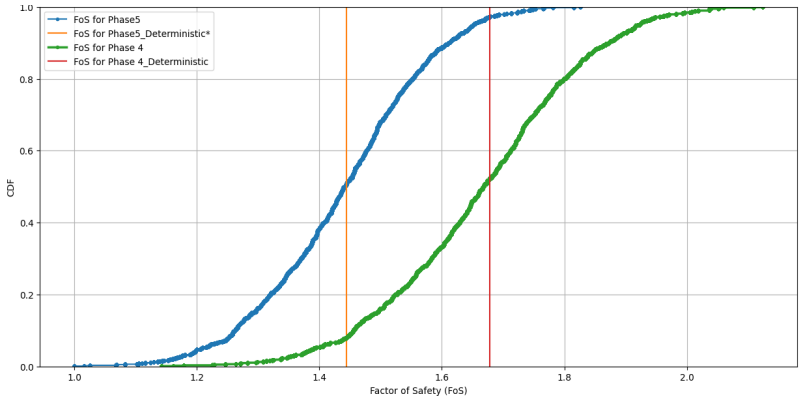

[COV 20%]

Figure 4.13: Cumulative distribution (%) of generated factor of safety in phase 4 and 5 under COV 10% and 20%. Vertical lines present a single value in deterministic design.

All provided results indicate that the likelihood of failure for COV 10% is as low as 0.017% indicating a reliable design for phase 4. However, the failure probability increased to 15% in same phase with COV 20%. In phase 5, the majority of cases were observed to yielding a FoS bellow the defined threshold. The generated factor of safety in COV 10% indicated to a probability of failure at 64% and slightly higher at 64.8% with considering to COV 20%.

It can be discussed that the results for the factor of safety show the similar impact of COVs combined with traffic load. it is evident that probabilistic approach have taken to account the variability in clay's cohesion and stiffness on the factor safety. As a result increasing variability in clay's strength related parameters lead to a decrease in geotechnical safety for the surrounding soil near to sheet pile wall. The combined effect of underestimated soil variability and the addition of traffic loads in phase 5 results in significantly unsafe soil behaviour (FoS lower than 1.5). In phase 5(COV 10%), at least 80% of the realizations fall into the unsafe zone, whereas in

phase 4, without the impact of traffic loads, geotechnical safety is maintained in most realizations.

It was found that a COV of 20% generated realizations that are more stretched towards either very unsafe or very safe outcomes, while a COV of 10% tends to concentrate in the middle of the CDF diagram. Notably, the effect of the surcharge load in phase 5 demonstrated a steeper line which indicate rapid change of soil's response to additional loads from the surface. The variability in factor of safety makes it easier to detect how quickly the overall response of the soil around the wall can vary with respect to the surcharge load and uncertain representative data. From a practical standpoint, the results revealed how uncertainty in site investigation can influence potential outcomes and underscore the importance of having adaptive designs to ensure geotechnical safety.

4.6 Combination of maximum bending moment with Factor of safety

The analysis of the influence of maximum bending moments on the safety factor reveals a consistent pattern across different phases of construction. In Phase 4, with a coefficient of variation (COV) of 10% and 20%, there was a higher frequency of observations with a safety factor greater than 1.5 compared to Phase 5 (see fig 4.14). The presence of traffic load in Phase 5 appears to increase the earth pressure due presence of weaker layers, consequently increasing the likelihood of surpassing critical load thresholds. The concentration of data points within the unsafe region during Phase 5 indicates a clear trend. As the maximum bending moment exceeds the 150 kNm/m mark in combination with possibly low shear strength, especially in the level near to toe of the wall, a considerable number of safety factor observations begin to decline, signaling a transition towards a high-risk zone. Moreover, the blue trend line in the plot reinforces this observation, illustrating a decrease in the safety factor as the maximum bending moment exerted on the sheet pile wall increases. Notably, in figure 4.15 several observations approach the 400 kNm/m level, approaching the wall's bending moment capacity of 500 kNm/m. At this interval, the soil's response is critically compromised, evidenced by the increased maximum bending moments nearing the wall's design limits.

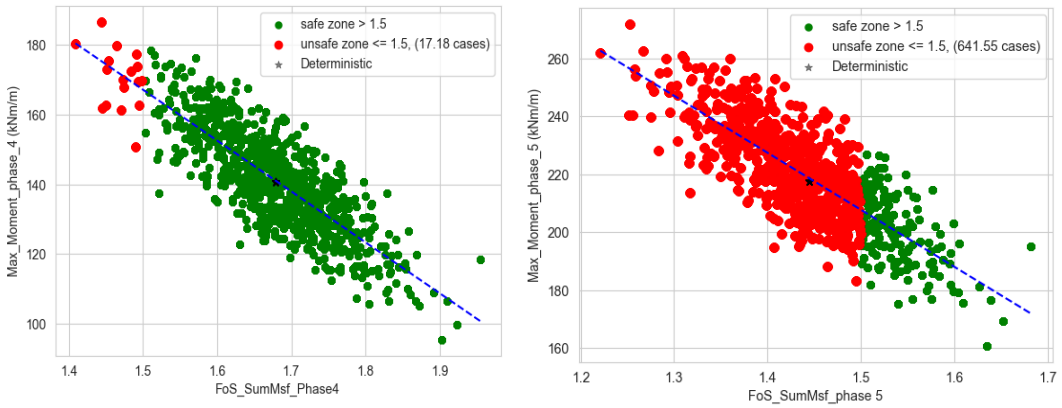

Figure 4.14: The interaction of maximum bending moment with soil's factor of safety under COV 10% in phase 4 and 5.

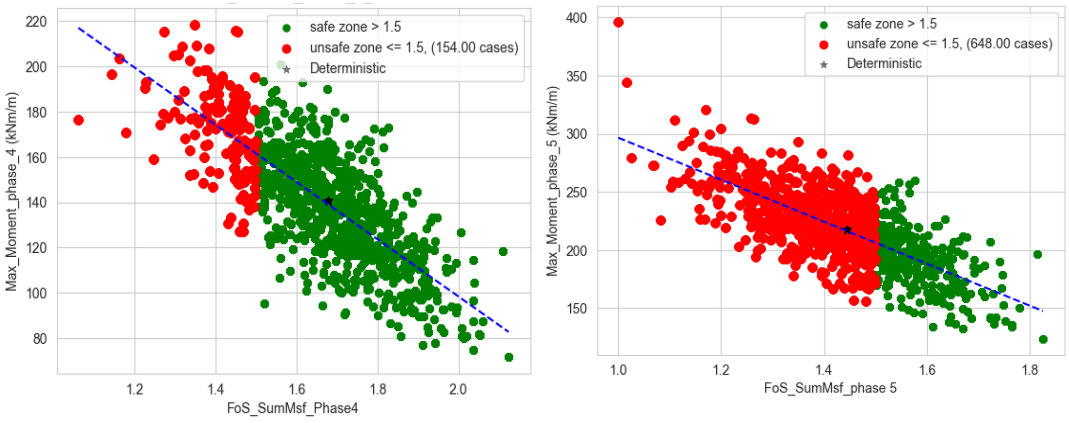

Figure 4.15: The interaction between maximum bending moment and soil's factor of safety under COV 20% in phase 4 and 5.

4.7 Combination of waler force with Factor of safety

To interpret the interplay between structure elements, variation in clay's stiffness, cohesion and the factor of safety, a series of scatter plots were generated. The purpose of plotting of each studied structure performance such as wall's bending moment, waler force and wall deflection is that to demonstrate how these factors impact the performance of the soil around the sheet pile wall. These plots, as illustrated in the figures 4.16 and 4.17, categorize observations into a 'safe zone'(highlighted in green), where as mentioned before the factor of safety is above 1.5 and an 'unsafe zone' (indicated by red points), where the FoS falls below 1.5. These zones are evaluated under both a 10% and a 20% Coefficient of Variation (COV).
In Phase 4, the distribution of safe observations under both COV 10% and COV 20% indicates a greater concentration of data points within the safe zone, beyond the FoS threshold of 1.5. Specifically, 17 observations were located in the unsafe zone at a COV of 10%, and this number has increased to 154 under a COV of 20%, demonstrating a smaller subset compared to the safe zone. The spread of anchor forces suggests that forces ranging from -100 to nearly -130 kN correlate with the safe zone, whereas forces extending from -130 kN/m to -180 kN/m align with the unsafe zone.
When considering the combination of anchor force and the safety factor for deterministic design, marked by a black star, it is revealed that the deterministic case consistently falls within the unsafe zone for all COVs 10% and 20% in Phase 5. This insight underscores the importance of incorporating variability into design practices to ensure geotechnical structures are reliably secure under a range of potential conditions.

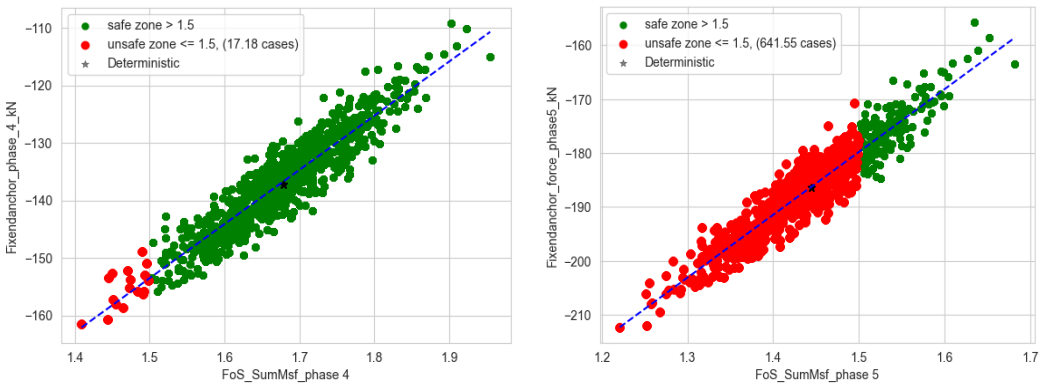

Figure 4.16: The impact of anchor load on soil factor of safety for COV 10% in phase 4(excavation) and phase 5(traffic load).

In Phase 5, a considerable number of observations fall into the unsafe zone for both COV values of 10% and 20%, as it is indicated in the figures. This trend highlights the significant impact that traffic loads have on the stability of retaining structures. It is apparent that there is a positive linear relationship between anchor force and the factor of safety, demonstrating that as traffic loads are applied, a majority of the realizations transition into the unsafe zone. Furthermore, the scope of force within the unsafe zone has expanded, with some observations exceeding -325 kN. This suggests that under the influence of traffic loads, the retaining structures are subjected to considerably advanced forces, which in turn reduces the factor of safety dramatically, pushing the system towards a higher likelihood of failure.

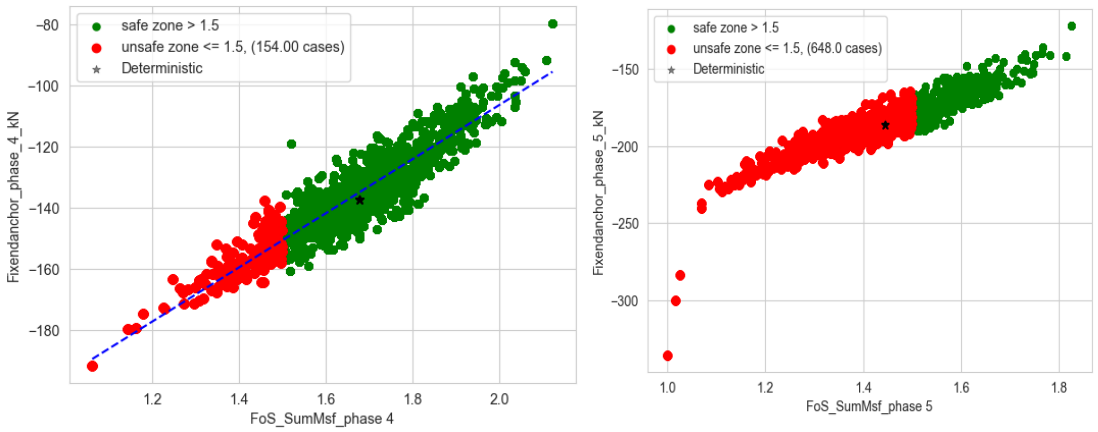

Figure 4.17: The impact of anchor load on soil factor of safety for COV 20% in phase 4(excavation) and phase 5(traffic load).

4.8 Combination of wall deflection (Ux) with Factor of safety

Lastly, the scatter plots in figure 4.18 provide an essential insight into the relationship between wall deflection and soil stability during the only construction phase 4. The distribution of data points effectively captures the variability in soil response as influenced by the coefficient of variation (COV). An important observation from these plots is that under a COV 10%, few realizations fell below the selected safety factor threshold. However, when the COV was escalated to 20%, there was a substantial increase in the number of realizations deemed unsafe, increasing by a factor of nine. This stark increase emphasizes the sensitivity of soil stability to the COV, as COV values goes up to a shift toward lower safety factors. The results further indicate that wall deflections extending up to 8 cm are within the bounds of safety, maintaining a factor of safety above the critical value of 1.5, regardless of COV

values.

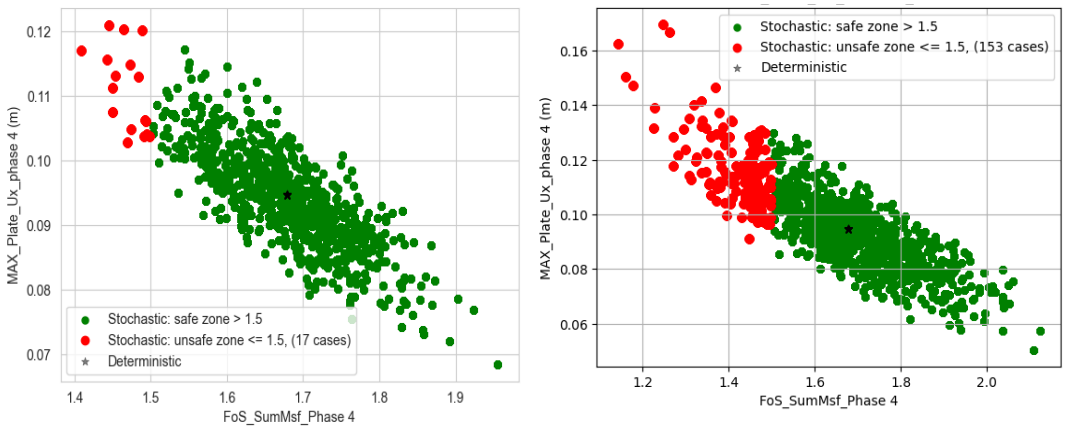

Figure 4.18: impact of wall deflection on factor of safety under COVs 10% and 20% (only phase 4)

The analysis of all combined cases indicates vividly that the factor of safety must be enhanced to achieve a more robust design in phase 5. This could be accomplished either by eliminating traffic behind the wall during construction or by increasing lateral support. For instance, the response of the wall to the loads generated by traffic was inadequate to maintain the required geotechnical safety margin in the majority of cases. Additionally, the combined cases confirm that the geotechnical limit is violated in most realizations in phase 5, considering both COVs.

Overall, all realizations and their interaction with the factor of safety suggest that the design must be more robust to minimize the high risk of unsafe geotechnical behaviour, particularly with regarding to 20 kPa traffic load, which could increase the probability of failu. The 2000 simulations provide a realistic assessment of the final design, capturing all potential complications to ensure more stable and safe geotechnical structures. It was evident that waler force showed almost linear behaviour with positive trend in phase 4 by considering to soil variability. However, this linear behaviour changed into non-linear by adding higher uncertainty in clay's stiffness and cohesion. The linkage effect of waler and FoS demonstrated an example of non-linear behaviour of soil when waler force surpassed -250 kN/m, the safety factor decreased non-linearly and reached to 1.00.
These findings highlight that deterministic soil inputs, which consider single result(shown by black star), tend to offer overly optimistic outcomes. In contrast, probabilistic designs present a range of outcomes, enabling geotechnical engineers to evaluate a more realistic safety margin.

5
Conclusion

The conclusion of this thesis reflects the most important findings from various analyses conducted based on a real case in Gothenburg. Fully probabilistic analysis was applied using PLAXIS 2D to simulate the influence of uncertainty in two key input variables: undrained shear strength and stiffness of clay. This approach was used to assess the performance of embedded sheet pile walls in deep excavations. The results provide critical insights into quantifying the impact of soil variability on bending moments, waler forces, wall deflections, geotechnical factors of safety, and the interaction between wall performance and geotechnical safety factors.
It is important to note that this thesis demonstrate that it is possible to perform fully probabilistic analysis with a normal personal laptop by integrating Python scripts with PLAXIS 2D to achieve a reliability index of three. However, reaching higher reliability indices requires significantly more computational time and perhaps more powerful computer. Furthermore, the provided results demonstrated the limitations and advantages of probabilistic design compared to traditional design practices were highlighted. The paragraphs below summarize the main conclusions drawn from this thesis.

- The findings highlighted the limitations of the traditional design approach, which failed to capture the structural and soil behavior caused by soil variability. While hand calculations using partial methods provided a single result, the probabilistic method employed in Monte Carlo simulations with PLAXIS 2D successfully captured the non-linear behavior of structural performance. This was achieved by using an elastoplastic material model in PLAXIS 2D, which accurately represented the entire behavior of the structure. In contrast, hand calculations assumed the behavior of the structure to be purely plastic, relying on partial factor methods.

- Simplified probabilistic analyses presented uncertainty-based designs that accounted for system-level performance, different failure mechanisms, and the probability of failure, rather than simply indicating whether failure occurs. Traditional hand calculations offered cheaper designs by not quantifying uncertainty in input variables. In contrast, probabilistic designs adapted to the level of uncertainty in soil properties and considered the elastoplastic behavior of the structure, resulting in more expensive but statistically insightful designs. Additionally, by capturing stress, strain, structural behaviors, and probabilities of failure, probabilistic design can be recognized as an important tool for geotechnical engineers to improve the geotechnical design.

- However, the limitations of the provided results can be influenced by the use of the simplified Mohr-Coulomb soil model in PLAXIS 2D and the number of realizations based on the target risk level. Attention must be paid to these factors to ensure the reliability and applicability of the results.

- The provided results highlighted that adding uncertainty in clay's stiffness and undrained shear strength significantly varied the structural responses. When 20% uncertainty was applied to these variables, it resulted in larger bending moments, higher wall deflections, higher waler forces, and lower factors of safety, which aligned with past studies. The application of a COV of 20% increased the spread of outcomes related to structural performance, leading to a decrease in the reliability of the design.

- In contrast, a COV of 10% presented a narrower range of outcomes, indicating better predictability and reliability. The influence of uncertainty combined with traffic load greatly increased the unreliability of the design. The findings indicated that selecting a coefficient of variation of 20% is appropriate for increasing conservatism in design, as it accounts for a wider range of potential scenarios and ensures safety under highly variable conditions. Conversely, for assessing structural performance within a narrower and more predictable range, a COV of 10% is recommended.

- The findings demonstrated that among all studied performance metrics, the performance of the waler, wall deflection, and soil around the wall were highly sensitive to higher levels of uncertainty and traffic loads.

- The analysis of 2000 realizations with different levels of uncertainties showed that deterministic designs consistently required an increase in the factor of safety, as all results were below Eurocode 7's predefined partial factor of 1.5. However, it should be noted that using a factor of 1.5 is too conservative to meet the minimum requirement for a reliability index of 3.

- Finally, finite element analysis demonstrated the significant negative impact of traffic loads behind the wall on waler forces and the factor of safety, especially when combined with a COV of 20%. Notably, the geotechnical factor of safety declined significantly in phase 5. The effect of traffic load on structural elements and their linkage with the factor of safety revealed that having a 20 kPa line load behind the wall can greatly decrease the robustness of the design and increase the risk of failure. This highlights the importance of further investigating the real coefficient of variation in Gothenburg to develop better strategies for managing traffic loads behind the wall.

6
Recommendations

The responses of structures and soil around the retaining wall with respect to two uncertainty levels of 10% and 20% have been studied. It was shown that the performance of the structure under 20% uncertainty was not sufficient. It is recommended that identifying and measuring the real coefficient of variation of Gothenburg clay and applying it to probabilistic analysis can significantly increase the quality and reliability of geotechnical design.

Furthermore, there is a large difference between hand calculations and mean values determined by probabilistic design in PLAXIS 2D, which requires further investigation to identify the main reasons. However, based on the results provided in this thesis, it is suggested to use these values in design (considering traffic load) to achieve a reliability index of three. The design value of bending moment is recomended to be at least 289 kN/m (hand calculation = 214 kN/m), the design value of waler/strut force is 229 kN/m (hand calculation = 128 kN/m), and the wall deflection in the horizontal direction is 8 cm.

Bibliography

[1] Andrew, L. (2012). Using numerical analysis with geotechnical design codes. Modern Geotechnical Design Codes of Practice: Implementation, Application and Development, 1, 157.

[2] Brinkgreve, R. (2007). PLAXIS 2D. Version 8.5 finite-element code for soil and rock analyses: Complete set of manuals. Netherlands.

[3] Brinkgreve, R., Kumarswamy, S., Swolfs, W., Waterman, D., Chesaru, A., & Bonnier, P. (2016). PLAXIS 2016. PLAXIS bv, the Netherlands, 1-16.

[4] Ching, J., & Phoon, K.-K. (2015). Constructing multivariate distributions for soil parameters. Risk and reliability in geotechnical engineering, 3-76.

[5] Ching, J., Phoon, K.-K., & Wu, T.-J. (2016). Spatial correlation for transformation uncertainty and its applications. Georisk: Assessment and Management of Risk for Engineered Systems and Geohazards, 10(4), 294-311.

[6] Damians, I., Bathurst, R., Josa, A., & Lloret, A. (2015). Numerical analysis of an instrumented steel-reinforced soil wall. International Journal of Geomechanics, 15(1), 04014037.

[7] Duncan, J. M. (2000). Factors of safety and reliability in geotechnical engineering. Journal of geotechnical and geoenvironmental engineering, 126(4), 307-316.

[8] Fenton, G. A., Naghibi, F., Dundas, D., Bathurst, R. J., & Griffiths, D. V. (2015). Reliability-based geotechnical design in 2014 Canadian highway bridge design code. Canadian geotechnical journal, 53(2), 236-251.

[9] Hicks, M. A. (2012). An explanation of characteristic values of soil properties in Eurocode 7. Modern geotechnical design codes of practice: Implementation, application and development, 1, 36-45.

[10] Honjo, Y. (2008). Monte Carlo simulation in reliability analysis. In Reliability-based design in geotechnical engineering (pp. 181-203). CRC Press.

[11] Kempfert, H.-G. (2006). Excavations and foundations in soft soils. Springer.

[12] Kulhawy, F. H. (1992). On the evaluation of static soil properties. Stability and performance of slopes and embankments II.

[13] Kullingsjö, A., Fredriksson, A., Ryner, A., & Stille, H. (2018). Sponthandboken 2018. In: Stockholm.

[14] Labuz, J. F., & Zang, A. (2014). Mohr–Coulomb failure criterion. In The ISRM Suggested Methods for Rock Characterization, Testing and Monitoring: 2007-2014 (pp. 227-231). Springer.

[15] Lees, A. (2016). Geotechnical finite element analysis: a practical guide. ICE publishing.

[16] Low, B.-K. (2018). Reliability-based design: practical procedures, geotechnical examples, and insights. In Risk and reliability in geotechnical engineering (pp. 385-424). CRC Press.

[17] Low, B. K. (2008). Practical reliability approach using spreadsheet. In Reliability-Based Design in Geotechnical Engineering (pp. 146-180). CRC Press.

[18] Moormann, C. (2004). Analysis of wall and ground movements due to deep excavations in soft soil based on a new worldwide database. Soils and foundations, 44(1), 87-98.

[19] Orr, T. L., & Breysse, D. (2008). Eurocode 7 and reliability-based design. In Reliability-based design in geotechnical engineering (pp. 310-355). CRC Press.

[20] Ou, C.-Y. (2021). Fundamentals of deep excavations. CRC Press.

[21] Phoon, K.-K., & Ching, J. (2015). Risk and reliability in geotechnical engineering. CRC Press Boca Raton, FL, USA.

[22] Phoon, K.-K., & Kulhawy, F. H. (1999a). Characterization of geotechnical variability. Canadian geotechnical journal, 36(4), 612-624.

[23] Phoon, K.-K., & Kulhawy, F. H. (1999b). Evaluation of geotechnical property variability. Canadian geotechnical journal, 36(4), 625-639.

[24] Phoon, K.-K., & Kulhawy, F. H. (2008). Serviceability limit state reliability-based design. In Reliability-based Design in Geotechnical Engineering (pp. 356-396). CRC Press.

[25] Phoon, K., & Ching, J. (2015). Characterization of geotechnical variability—A multivariate perspective. Comput. Methods Recent Adv. Geomech, 61-70.

[26] Sert, S., Luo, Z., Xiao, J., Gong, W., & Juang, C. H. (2016). Probabilistic analysis of responses of cantilever wall-supported excavations in sands considering vertical spatial variability. Computers and Geotechnics, 75, 182-191.

[27] Spry, M., Kulhawy, F., & Grigoriu, M. (1988). Reliability-based foundation design for transmission line structures: Volume 1, Geotechnical site characterization strategy.

[28] Wang, Y., Schweckendiek, T., Gong, W., Zhao, T., & Phoon, K.-K. (2016). Direct probability-based design methods. In Reliability of geotechnical structures in ISO2394 (pp. 211-244). CRC Press.

[29] Zhang, J., Xiao, T., Ji, J., Zeng, P., & Cao, Z. (2023). Geotechnical Reliability Analysis: Theories, Methods and Algorithms. Springer Nature.

A

Further Study

- Examine the influence of Gothenborg's coeficient of variation and environmental factors, such as seasonality with probabilistic based design to provide a broader understanding of influencing factors during the geotechnical design process.

- Predict wall deflection using machine learning methods and incorporate large datasets generated by multiple random soil and structural variables to reduce computational time and increase effectiveness in the design process.

- Evaluate structural performance by incorporating the consolidating behavior of soft clay using more advanced soil models. Explore time-dependent behavior combined with higher coefficients of variation and higher reliability indices to provide more robust designs in complex situations.

A

Appendix

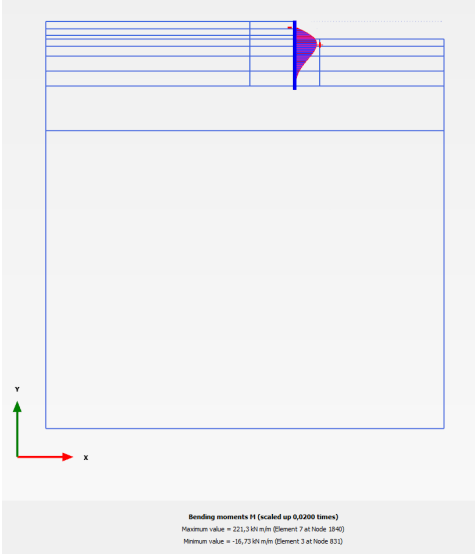

Figure A.1: Result of maximum bending moment in phase 5 by medium mesh.

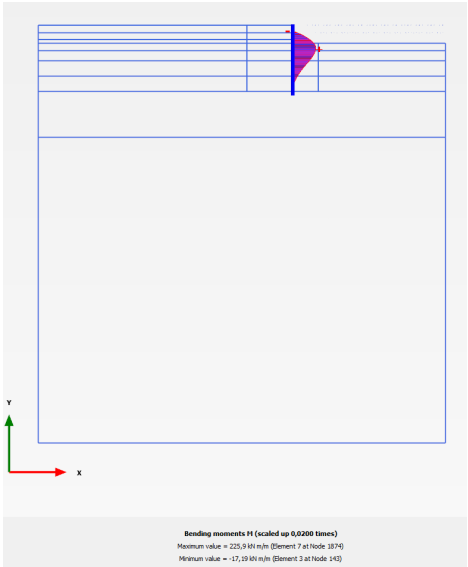

Figure A.2: Result of maximum bending moment in phase 5 by fine mesh.

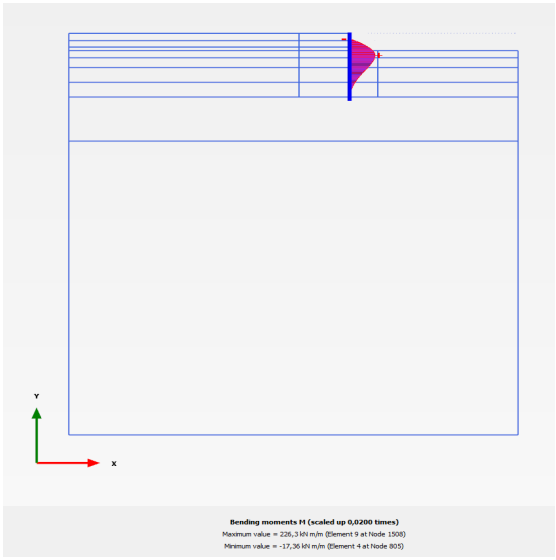

Figure A.3: Result of maximum bending moment in phase 5 by very fine mesh.

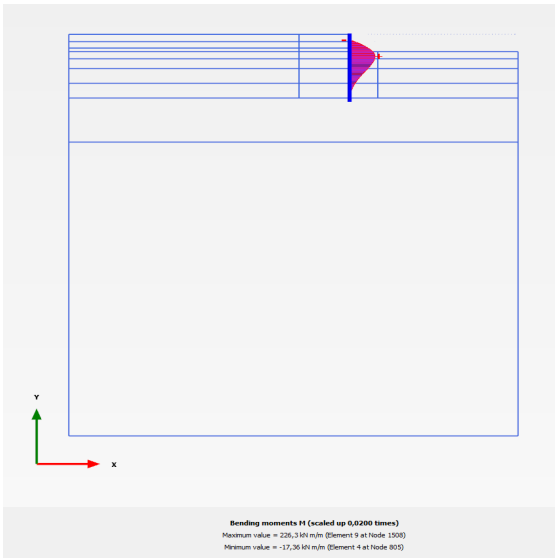

Figure A.4: Result of maximum bending moment in phase 5 by very fine mesh.

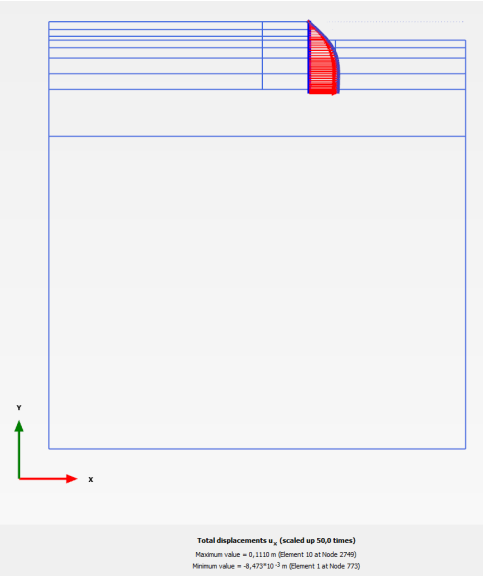

Figure A.5: Result of maximum wall deflection in phase 5 by medium mesh.

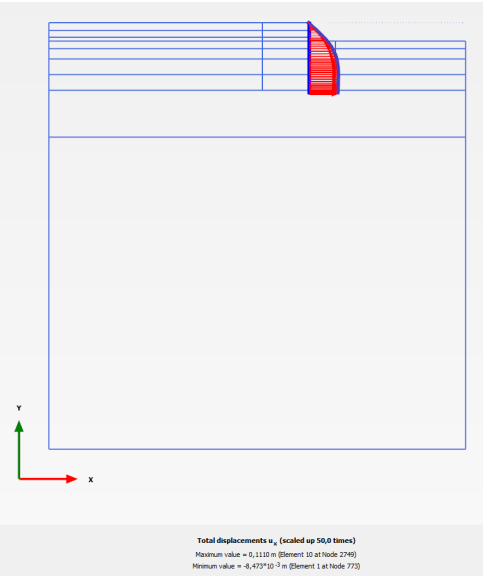

Figure A.6: Result of maximum wall deflection in phase 5 by fine mesh.

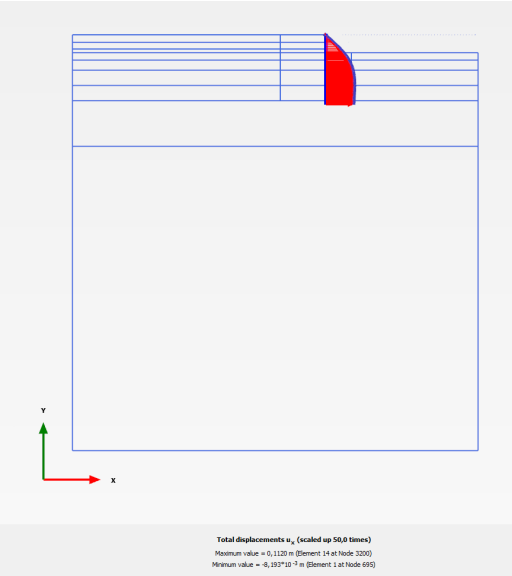

Figure A.7: Result of maximum wall deflection in phase 5 by very fine mesh.